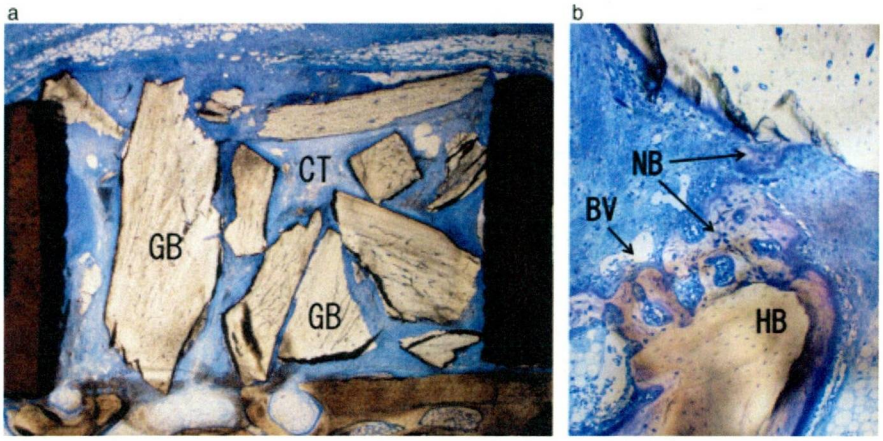

Fig. 6. Large bone grafted site at 2 weeks. (a) Grafted bone (GB) almost preserved its original shape. In the interspace of the GB, fibrous connective tissue (CT) was observed. Magnification × 2.5. (b) High-magnification image of (a). In the region close to the host bone (HB), blood vessels (BV) were found, and new bone (NB) formation occurred from the host bone surface to the GB surface. Magnification × 25.

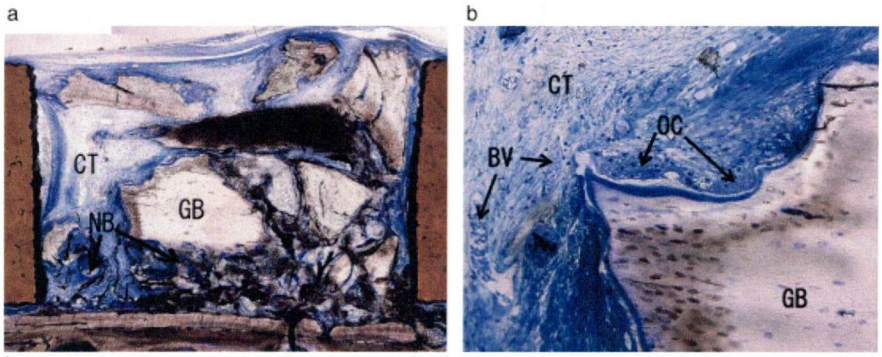

Fig. 7. Large bone grafted site at 4 weeks. (a) The center of grafted bone (GB) retained its original form. Fibrous connective tissue (CT) was observed around GB. A large amount of new bone (NB) was formed from the host bone surface to the GB surface. Magnification × 2.5. (b) High-magnification image of (a). Howship's lacunae with osteoclast-like cells (OC) were found at the surface of GB. Fibrous connective tissue and blood vessels (BV) were observed around the GB. Magnification × 40.

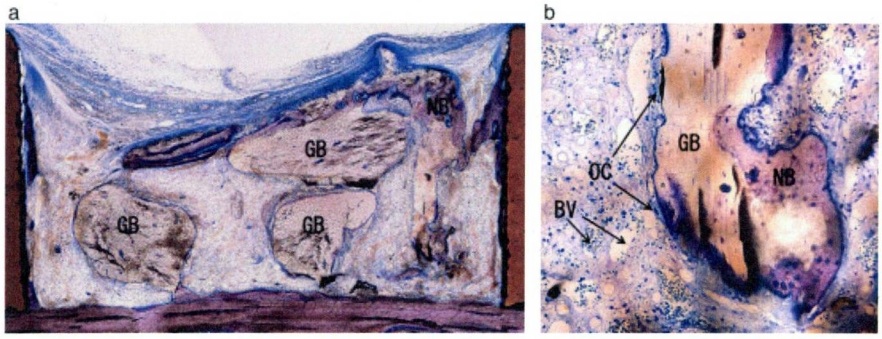

Fig. 8. Large bone grafted site at 8 weeks. (a) Newly formed bone (NB) was observed around the grafted bone (GB). GB was covered by NB, and many osteocytes were observed. Magnification × 2.5. (b) High-magnification image of (a). Osteoclast-like cells (OC) were observed on the surface of the GB. Around this bone architecture, many blood vessels (BV) were observed. Magnification × 40.

with 850–1000 μm particles yielded favorable results than the 250–500 μm particles in human periodontal defects (Fucini et al. 1993). Unmilled bone particle had more osteoblast than milled and drilled bone (Springer et al. 2004). In another study, application of 250–500 μm particle β-tricalcium phosphate particles exhibited more advantages in terms of bone formation than the 100–250 μm-sized particles (Murai et al. 2006). These results agree with the present study. However, the observations about particle size varied. In a rabbit autogenous graft defect model, there was no difference between the non-graft control, collected debris and particles collected by a manual bone crusher (Coradazzi et al. 2007). In addition, no significant difference was detected between the control defect and two sizes of β-tricalcium phosphate particles, 500–1000 and 1000–2000 μm, applied to a cynomolgus monkey mandible defect model (Kuroki et al. 2008). In these two studies, augmentation material was applied to the defect model, which was different from the chamber model in other studies, and is considered not suitable for confirming the augmentation potency. Hence, it would appear that application of large graft materials is preferable for bone augmentation. However, Pallesen et al. (2002) reported that 0.5–2.0 mm^3 particle autogenous bone exhibited more newly formed bone than 10 mm^3 in a rabbit cranial defect model. Thus, excessively large particles applied to a bone defect might have lower augmentation ability.

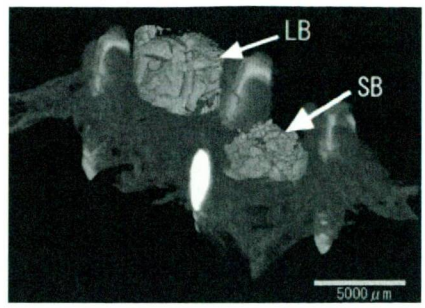

Fig. 9. Extracted image of bone-grafted site with micro-computed tomography (micro-CT). Both small bone (SB)- and large bone (LB)-grafted sites were extracted with micro-CT (grafted site image at 4 weeks).

The SB groups showed a considerable reduction of bone volume in the upper half of the chamber. The bone volumes of the upper half were 50.2%, 45.1%, 25.8% and 18.1% at 1, 2, 4 and 8 weeks, respectively. For this reason, BH of SB decreased at all experimental time points. Advanced biodegradability of small-sized grafted bone is considered to be responsible for these results. In contrast, LB could maintain the original shape of grafted bone in the upper half of the chamber; thus, BH was preserved during the entire period. Although the biodegradability of a bone substitute is

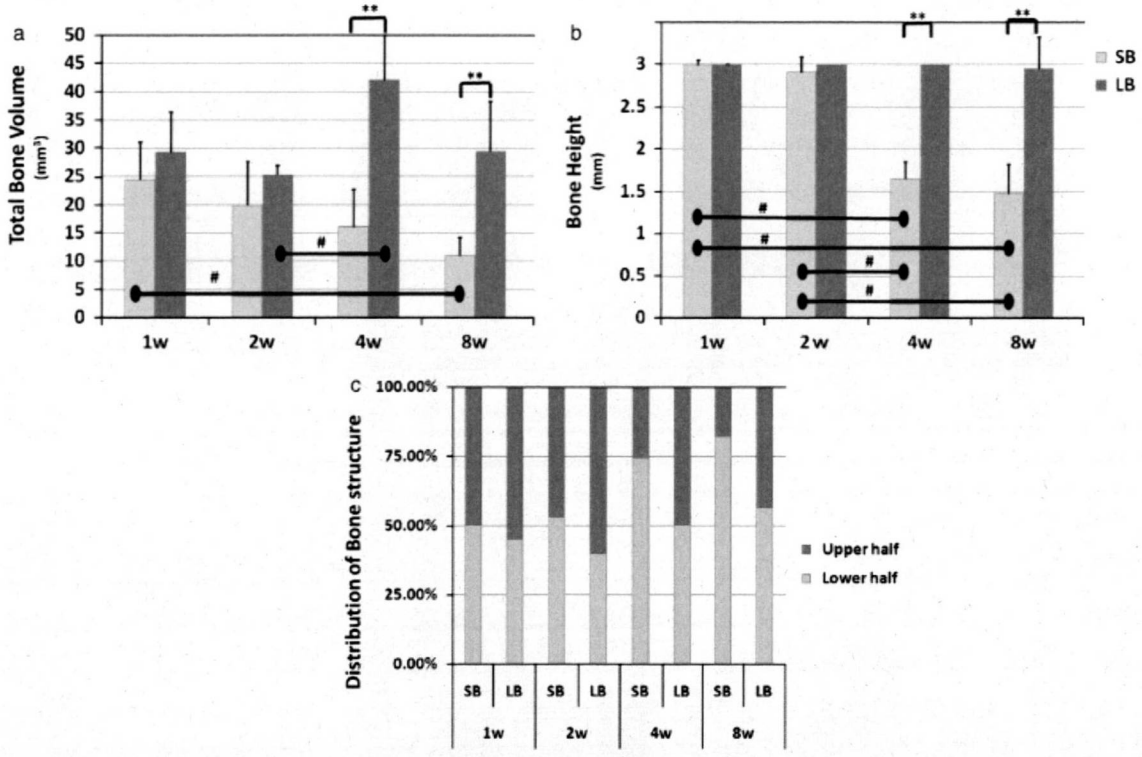

Fig. 10. Micro-computed tomography analysis. (a) Total bone volume change. Comparison between two groups – Mann–Whitney test, $^{**}P<0.01$; comparison within each group – non-parametric multiple comparison test, $^{\#}P<0.05$. Error bar indicates 95% confidence interval. (b) Bone height change. Comparison between two groups – Mann–Whitney test, $^{**}P<0.01$; comparison within each group – non-parametric multiple comparison test, $^{\#}P<0.05$. Error bar indicates 95% confidence interval. (c) Distribution of bone structure. Notably, bone volume reduction of the upper half was observed in small bone (SB) models. In contrast, large bone (LB) models exhibited no dramatic change.

thought to be very important, taking into account the volumetric augmentation ability, morphological stability is essentially required.

Clinically, autogenous bone is believed to be the gold standard for bone augmentation. However, the augmentation ability could differ with particle size. The present study indicates that small autogenous bone debris would be easily resorbed, having a poor outcome for augmentation. Therefore, to achieve sufficient bone augmentation, small autogenous bone debris should be applied in combination with a slow or a non-resorbable bone substitute. On the other hand, LB exhibited favorable augmentation with morphological stability. However, the osteogenesis in the interspace of grafted LB was limited, and newly trabecula formation progressed slowly throughout the entire experimental period. Therefore, to enhance osteogenesis in the interspace, application of SB might be effective.

Within the limitations of the present study, it is concluded that SB decreased to 51.3% and 51.0% of the initial volume and height, respectively, and LB could maintain the volume and height at 8 weeks in this augmentation model. SB follows smooth osteogenic process, whereas it is not effective in volume augmentation. However, LB is superior to SB in augmentation ability, although further studies are needed to evaluate the longitudinal bone augmentation condition.

References

Boronat-Lopez, A., Carrillo, C., Peñarrocha, M. & Peñarrocha-Diago, M. (2009) Immediately restored dental implants for partial-arch applications: a study of 12 cases. *Journal of Oral and Maxillofacial Surgery* **67**: 195–199.

Boyne, P. & James, R. (1980) Grafting of the maxillary sinus floor with autogenous marrow and bone. *Journal of Oral Surgery* **38**: 613–616.

Chiapasco, M., Consolo, U., Bianchi, A. & Ronchi, P. (2004) Alveolar distraction osteogenesis for the correction of vertically deficient edentulous ridges: a multicenter prospective study on humans. *International Journal of Oral & Maxillofacial Implants* **19**: 399–407.

Coradazzi, L., Garcia, I.J. & Manfrin, T. (2007) Evaluation of autogenous bone grafts, particulate or collected during osteotomy with implant burs: histologic and histomorphometric analysis in rabbits. *International Journal of Oral & Maxillofacial Implants* **22**: 201–207.

Ferrigno, N., Laureti, M., Fanali, S. & Grippaudo, G. (2002) A long-term follow-up study of non-submerged ITI implants in the treatment of totally edentulous jaws. Part I: ten-year life table analysis of a prospective multicenter study with 1286 implants. *Clinical Oral Implants Research* **13**: 260–273.

Fucini, S., Quintero, G., Gher, M., Black, B. & Richardson, A. (1993) Small versus large particles of demineralized freeze-dried bone allografts in human intrabony periodontal defects. *Journal of Periodontology* **64**: 844–847.

Fugazzotto, P. & Vlassis, J. (2007) Report of 1633 implants in 814 augmented sinus areas in function for up to 180 months. *Implant Dentistry* **16**: 369–378.

Hämmerle, C., Jung, R., Yaman, D. & Lang, N. (2008) Ridge augmentation by applying bioresorbable

membranes and deproteinized bovine bone mineral: a report of twelve consecutive cases. *Clinical Oral Implants Research* **19**: 19–25.

Jemt, T. & Lekholm, U. (2003) Measurements of buccal tissue volumes at single-implant restorations after local bone grafting in maxillas: a 3-year clinical prospective study case series. *Clinical Implant Dentistry & Related Research* **5**: 63–70.

Johansson, B., Grepe, A., Wannfors, K. & Hirsch, J. (2001) A clinical study of changes in the volume of bone grafts in the atrophic maxilla. *Dentomaxillofacial Radiology* **30**: 157–161.

Kihara, H., Shiota, M., Yamashita, Y. & Kasugai, S. (2006) Biodegradation process of alpha-TCP particles and new bone formation in a rabbit cranial defect model. *Journal of Biomedical Material Research B Applied Biomaterial* **79**: 284–291.

Kuroki, H., Toda, I. & Suwa, F. (2008) Experimental study of bone defect repair process with different sizes of β-TCP granules. *Journals of Japanese Society of Oral Implantology* **21**: 21–31.

Lustmann, J. & Lewinstein, I. (1995) Interpositional bone grafting technique to widen narrow maxillary ridge. *International Journal of Oral & Maxillofacial Implants* **10**: 568–577.

Moy, P., Lundgren, S. & Holmes, R. (1993) Maxillary sinus augmentation: histomorphometric analysis of graft materials for maxillary sinus floor augmentation. *Journal of Oral and Maxillofacial Surgery* **51**: 857–862.

Murai, M., Sato, S., Fukase, Y., Yamada, Y., Komiyama, K. & Ito, K. (2006) Effects of different sizes of beta-tricalcium phosphate particles on bone augmentation within a titanium cap in rabbit calvarium. *Dentistry Material Journal* **25**: 87–96.

Pallesen, L., Schou, S., Aaboe, M., Hjørting-Hansen, E., Nattestad, A. & Melsen, F. (2002) Influence of particle size of autogenous bone grafts on the early stages of bone regeneration: a histologic and stereologic study in rabbit calvarium. *International Journal of Oral & Maxillofacial Implants* **17**: 498–506.

Rodriguez, A., Anastassov, G., Lee, H., Buchbinder, D. & Wettan, H. (2003) Maxillary sinus augmentation with deproteinated bovine bone and platelet rich plasma with simultaneous insertion of endosseous implants. *Journal of Oral and Maxillofacial Surgery* **61**: 157–163.

Scabbia, A. & Trombelli, L. (2004) A comparative study on the use of a HA/collagen/chondroitin sulphate biomaterial (Biostite) and a bovine-derived HA xenograft (Bio-oss) in the treatment of deep intra-osseous defects. *Journal of Clinical Periodontology* **31**: 348–355.

Springer, ING., Terheyden, H., Geiß, S., Härle, F., Hedderich, J. & Açil, Y. (2004) Particulated bone grafts – effectiveness of bone cell supply. *Clinical Oral Implants Research* **15**: 205–212.

Turunen, T., Peltola, J., Yli-Urpo, A. & Happonen, R. (2004) Bioactive glass granules as a bone adjunctive material in maxillary sinus floor augmentation. *Clinical Oral Implants Research* **15**: 135–141.

Walsh, W., Vizesi, F., Michael, D., Auld, J., Langdown, A., Oliver, R., Yu, Y., Irie, H. & Bruce, W. (2008) Beta-TCP bone graft substitutes in a bilateral rabbit tibial defect model. *Biomaterials* **29**: 266–271.

Widmark, G., Andersson, B. & Ivanoff, C. (1997) Mandibular bone graft in the anterior maxilla for single-tooth implants. Presentation of surgical method. *International Journal of Oral and Maxillofacial Surgery* **26**: 106–109.

Yildirim, M., Spiekermann, H., Biesterfeld, S. & Edelhoff, D. (2000) Maxillary sinus augmentation using xenogenic bone substitute material Bio-oss in combination with venous blood. A histologic and histomorphometric study in humans. *Clinical Oral Implants Research* **11**: 217–229.

Zaner, D. & Yukna, R. (1984) Particle size of periodontal bone grafting materials. *Journal of Periodontology* **55**: 406–409.

Myat Nyan
Daisuke Sato
Hidemichi Kihara
Tetsu Machida
Keiichi Ohya
Shohei Kasugai

Effects of the combination with α-tricalcium phosphate and simvastatin on bone regeneration

Authors' affiliations:
Myat Nyan, Daisuke Sato, Hidemichi Kihara, Tetsu Machida, Shohei Kasugai, Oral Implantology and Regenerative Dental Medicine, Tokyo Medical and Dental University, Tokyo, Japan
Myat Nyan, Shohei Kasugai, Center of Excellence Program for Frontier Research on Molecular Destruction and Reconstruction of Tooth and Bone, Tokyo Medical and Dental University, Tokyo, Japan
Keiichi Ohya, Section of Pharmacology, Department of Hard Tissue Engineering, Tokyo Medical and Dental University, Tokyo, Japan

Correspondence to:
Dr Myat Nyan
Oral Implantology and Regenerative Dental Medicine
Tokyo Medical and Dental University
1-5-45 Yushima, Bunkyo-ku
Tokyo 113-8549
Japan
Tel.: +81 3 5803 4664
Fax: +81 3 5803 4664
e-mail: myatnyan@gmail.com

Date:
Accepted 21 July 2008

To cite this article:
Nyan M, Sato D, Kihara H, Machida T, Ohya K, Kasugai S. Effects of the combination with α-tricalcium phosphate and simvastatin on bone regeneration. *Clin. Oral Impl. Res.* **20**, 2009; 280–287.
doi: 10.1111/j.1600-0501.2008.01639.x

Key words: α-TCP, BMP-2, bone formation, bone regeneration, simvastatin

Abstract

Background: Although local application of statins stimulates bone formation, high dose of simvastatin induces inflammation.

Objective: A study was conducted to test the hypothesis that maximum bone regeneration with less inflammation would be achieved by combining an optimal dose of simvastatin with α-tricalcium phosphate (α-TCP), which is an osteoconductive biomaterial capable of releasing the drug gradually.

Material and methods: Bilateral 5-mm-diameter calvarial defects were created in adult Wistar rats and filled with preparations of different doses of simvastatin (0, 0.01, 0.1, 0.25 and 0.5 mg) combined with α-TCP particles or left empty. The animals were sacrificed at 2, 4 and 8 weeks and analyzed radiologically and histologically. Half of the animals of 4 and 8 weeks were labeled with fluorescence dyes and histomorphometrically analyzed.

Results: Simvastatin doses of 0.25 and 0.5 mg caused inflammation of the soft tissue at the graft site whereas control and other doses did not. The micro-CT analysis revealed that the α-TCP with 0.1 mg simvastatin (TCP-0.1) group yielded significantly higher bone volumes than untreated control group at all three time points (249%, 227% and 266% at 2, 4 and 8 weeks, respectively). The percentage of defect closure, bone mineral content and bone mineral density were also higher in the TCP-0.1 group than in the other groups.

Conclusion: When combined with α-TCP particles, 0.1 mg simvastatin is the optimal dose for stimulation of the maximum bone regeneration in rat calvarial defects without inducing inflammation and it could be applied as an effective bone graft material.

With the expanding application of dental implant treatment to rehabilitate edentulous and partially edentulous patients, the demand for effective biomaterials for bone augmentation is increasing because there are disadvantages in autogenous bone grafting, such as donor site morbidity and limited availability of harvestable bone. In order to develop a bone graft with enhanced osteogenic properties, alloplastic bone substitutes have been combined with molecules, which enhance and/or induce new bone formation. Among these molecules, BMP-2 has especially shown its beneficial effects on bone regeneration. However, there are still some problems to be solved: such as short shelf life, inefficient delivery to target cells and high price (Einhorn 2003).

If pharmacological compounds can upregulate the intrinsic growth factors to stimulate bone growth, the strategy to combine such compounds with an osteoconductive bone substitute would be more cost-effective for bone regeneration. Topically applied simvastatin, a cholesterol-lowering drug, has been shown to

stimulate BMP-2 and VEGF mRNA expression in osteoblasts and promote bone growth over mouse calvaria (Mundy et al. 1999; Sugiyama et al. 2000; Garrett et al. 2001; Ohnaka et al. 2001; Thylin et al. 2002; Maeda et al. 2003; Ghosh-Choudhury et al. 2007). Other studies have reported that local application of statins induced bone growth in intact mandible, promoted bone regeneration in bone defects and tooth extraction sockets, and hastened fracture repair (Wong & Rabie 2003; Sato et al. 2005; Stein et al. 2005; Wong & Rabie 2005a, 2005b; Bradley et al. 2007; Garrett et al. 2007; Ozec et al. 2007; Sugiyama et al. 2007).

In our previous study, 1 mg simvastatin combined with calcium sulfate caused substantial bone regeneration in rat calvarial defects; however, considerable extent of soft-tissue inflammation was also observed at the site of application (Nyan et al. 2007). Other studies also reported that high doses of local simvastatin induced not only bone growth but also inflammation (Thylin et al. 2002; Stein et al. 2005). We hypothesized that the beneficial effects of simvastatin on bone regeneration with less inflammation could be achieved by combining an optimal dose of simvastatin with a bone substitute, which can gradually release the drug into the local bone environment. To test this hypothesis, we chose α-tricalcium phosphate (α-TCP) to combine with simvastatin. Calcium phosphate materials, such as hydroxyapatite and TCP, have been widely used as bone substitutes in orthopedic and maxillofacial surgery, as these materials show high biocompatibility and osteoconductivity. α-TCP has been shown to be a gradually degradable osteoconductive material (Wiltfang et al. 2002; Kihara et al. 2006). The purpose of this study was to evaluate bone regeneration by different doses of simvastatin in combination with α-TCP particles in rat calvarial defects and to determine the optimal dose of simvastatin for maximum bone regeneration with less inflammation.

Material and methods

Preparation of α-TCP and simvastatin combination

α-TCP particles with a diameter of 500–700 μm were obtained from Advance Co., Tokyo, Japan. Simvastatin (OHARA Pharmaceutical Co. Ltd, Koka, Shiga, Japan) was dissolved in ethanol and the solution was applied to the α-TCP particles by dropping under sterile conditions. As the α-TCP particles have numerous fine pores, the solution was uniformly and quickly distributed into the material. α-TCP particles containing the following doses of simvastatin were prepared: 0.01, 0.1, 0.25 and 0.5 mg per 14 mg α-TCP particles.

Anesthesia and surgical procedures

This study was approved by the institutional committee for animal experiments. Sixty-nine Wistar adult rats (16 weeks old) were used. The animals were anesthetized with a combination of ketamine–xylazine (40 and 5 mg/kg). The dorsal part of the cranium was shaved and prepared aseptically for surgery. A 20-mm-long incision in the scalp along the sagittal suture was made, and the skin, subcutaneous tissue and periosteum were reflected, exposing the parietal bones. Two full-thickness bone defects of 5 mm diameter were trephined in the dorsal part of the parietal bone lateral to the sagittal suture. A 5 mm trephine bur was used to create the defects under constant irrigation with sterile physiologic solution to prevent overheating of the bone edges. Care was taken during the surgical procedure to prevent damage to dura mater. In nine animals, both defects were left untreated to serve as negative control (Fig. 1a). In 45 animals, both defects were filled with 14 mg of α-TCP or α-TCP combined with 0.01, 0.1, 0.25 or 0.5 mg simvastatin (Fig. 1b), designated as TCP-0, TCP-0.01, TCP-0.1, TCP-0.25 or TCP-0.5 group, respectively ($n = 9$ for each group). In 15 animals, one defect was used to test each of the above materials whereas the other defect was left untreated to observe whether simvastatin from filled defect influenced the healing of contralateral unfilled defect (Fig. 1c). The periosteum and subcutaneous tissues were sutured in place using 4-0 Vicryl polyglactin suture (Ethicon Inc., NJ, USA) and the scalp with 4-0 silk (ELP Akiyma Co., Tokyo, Japan).

Animals were observed daily for any appearance of clinical signs of inflammation, photographed and recorded. For bone histomorphometrical analysis, 7 days and 1 day before sacrifice, calcein and tetracycline were injected, respectively, in half of the animals with particle-filled defects in 4-week and 8-week groups.

Tissue harvest and radiological analyses

Animals were sacrificed at 2, 4 and 8 weeks after the surgery. The skin was dissected and the defect sites were removed along with surrounding bone and soft tissues. Then, X-ray imaging was performed by a micro-CT scanner (InspeXio; Shimadzu Science East Corporation, Tokyo, Japan) with a voxel size of 70 μm/pixel. Tri/3D-Bon software (RATOC System Engineering Co. Ltd, Tokyo, Japan) was used to make a 3D reconstruction from the obtained set of scans. Out of the entire 3D data set, a cylindrical region of interest (ROI) with a diameter of 5 mm and a height that covered the entire thickness of the calvarial bone was selected for analysis. ROI was placed where the original defect was located as the margins were visually recognizable. Mask work was performed to binarize the α-TCP particles and new bone in the ROI separately according to different intensity values, as the former was more dense and radio-opaque than the latter. Then, the region of new bone was extracted from the whole binarized ROI by the logic operation work and the volume was measured. Percentage of defect closure was also calculated according to micro-CT images. After micro-CT analysis, bone mineral content (BMC) and bone mineral density (BMD) in the defect region of the 8-week samples were measured by dual-energy

Fig. 1. Bilateral 5 mm diameter rat calvarial defect model. (a) Empty control defects, (b) particle-filled defects filled with 14 mg of α-tricalcium phosphate particles, (c) unfilled defect contralateral to particle-filled defect to assess the influence of particle-filled defect.

X-ray absorptiometry for small animals (DXA-DCS-600; Aloka Co. Ltd, Tokyo, Japan).

Histological evaluation

After the radiological analyses, the specimens were fixed in 10% neutralized formalin for 1 week. The specimens from the animals that had not received vital labeling were decalcified in 5% formic acid for 2 weeks and then embedded in paraffin. Before the embedding procedure, an incision was made exactly through the middle of the bone defects to ensure that the microtome sections were made in the area of interest. Coronal sections of about 5 μm thickness were prepared, stained with hematoxylin–eosin and observed under an optical microscope.

Measurement of mineral apposition rate (MAR)

After harvesting and fixation procedures, the specimens were dehydrated in graded alcohol and embedded in the GMA/MMA resin. Five-micrometer-thick sections were cut coronally and unstained sections were observed under a fluorescent microscope for fluorochrome labeling. For MAR, interlabel distance was measured and the value was divided by the time interval between administrations of two vital markers. Then, the sections were stained with 0.1% toluidine blue for microscopic observation.

Statistical analysis

Data were first analyzed by one-way ANOVA. When this analysis suggested a significant difference between groups ($P<0.05$), the data were further analyzed by the Tukey *post hoc* multiple comparison tests.

Results

Macroscopic observation

All animals recovered well after surgery. No macroscopic infection of the wounds was noted. Side effects such as paralysis, convulsions, respiratory distress or signs of pain were not observed. In all animals of negative control, TCP-0, TCP-0.01 and TCP-0.1 groups, the soft tissue wounds healed uneventfully without showing clinical signs of inflammation. Animals in TCP-0.5 and TCP-0.25 groups revealed redness of the skin overlying the bone defects at 3 and 5 days, respectively. Localized area of swelling became evident over those areas from the following day in both groups. The inflamed areas proceeded to form ulceration and scabbing. The ulcers and scabs became reduced in intensity until 10 days. Generally, inflammation and scab formation were less intense in TCP-0.25 group and the soft tissue wounds healed 2–3 days earlier than those of TCP-0.5 group. At 2 weeks, the wounds showed complete soft tissue healing with the disappearance of swelling and/or scabbing.

Radiological observation

Control group

Scanty amount of new bone was formed in some areas along the margin of bone defect at 2 and 4 weeks (Fig. 2Ia and IIa). At 8 weeks, more new bone formation was observed with the thin layer of bone extending towards the center. However, there was no complete defect closure (Fig. 2IIIa).

TCP-0 and TCP-0.01 groups

Newly formed bone and grafted α-TCP particles could be easily differentiated as they revealed different radiopacity. At 2 and 4 weeks, only a small area of new bone was seen at the defect margins in both groups (Figs 2Ib and c and IIb and c). The bone formation became more evident at 8 weeks at the defect margins and around the TCP particles most of which appeared to be reduced in size but still present in the defect (Fig. 2IIIb and c).

TCP-0.1 group

At 2 weeks, the new bone was formed not only at the margin of the defect but also in between the α-TCP particles close to the

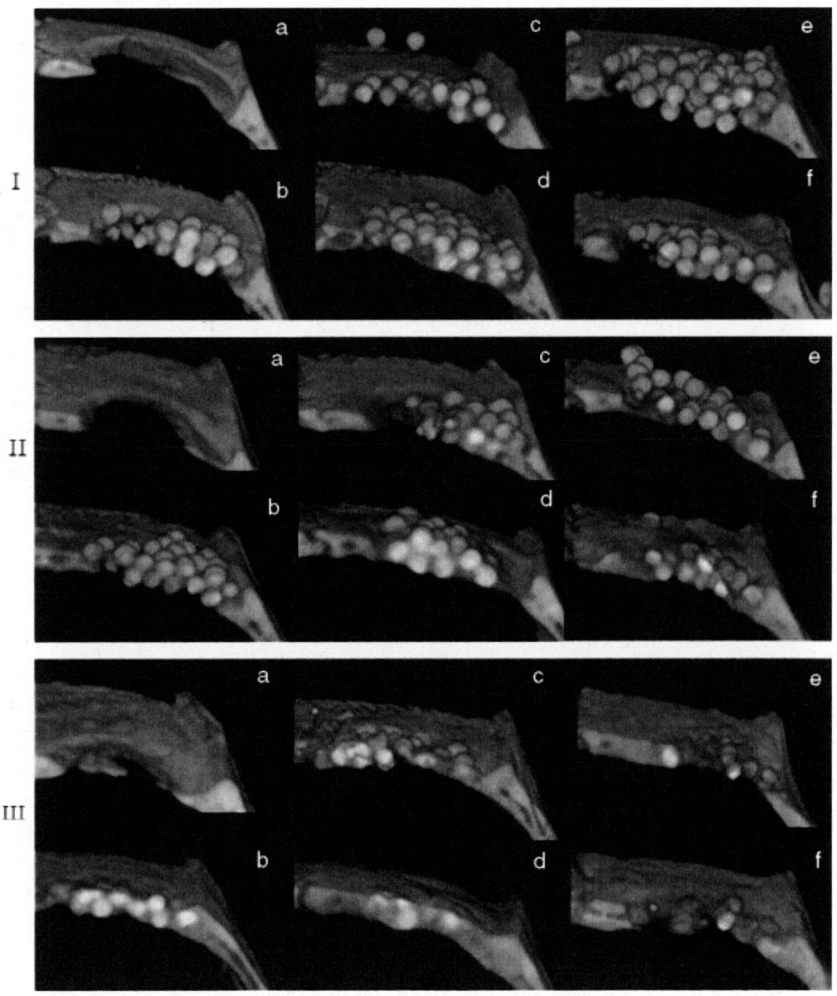

Fig. 2. Micro-CT images of bone defects at (I) 2 weeks, (II) 4 weeks and (III) 8 weeks. (a) Control, (b) TCP-0, (c) TCP-0.01, (d) TCP-0.1, (e) TCP-0.25, (f) TCP-0.5 groups. The images were trimmed to show the center of each defect. TCP, tricalcium phosphate.

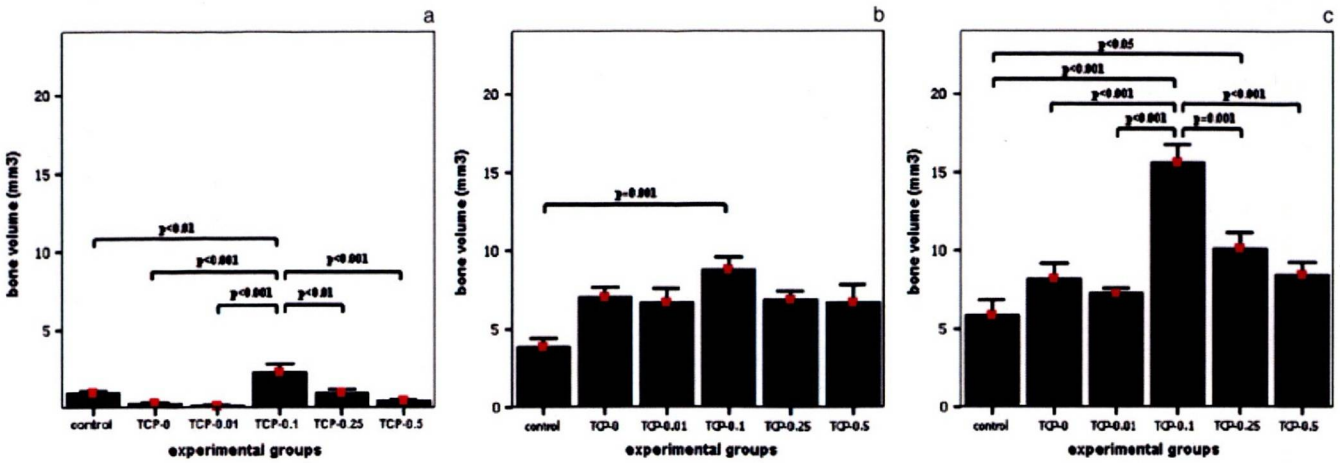

Fig. 3. Bone volume in the defect at (a) 2 weeks (b) 4 weeks and (c) 8 weeks. Bone volume was measured in micro-CT images three-dimensionally. Bars and error bars represent means and SEM, respectively. $n=7$ in each particle-filled group and $n=6$ in the control group at each time point. ANOVA 2 weeks ($F_{5,35}=10.655$, $P<0.0001$), 4 weeks ($F_{5,35}=3.861$, $P=0.007$), 8 weeks ($F_{5,35}=14.437$, $P<0.0001$).

dura mater (Fig. 2.Id). New bone continued to form between the defect margin and the α-TCP particles at 4 weeks. Bone had also penetrated in between the particles at the center of defect and resulted in almost a complete 3D closure of the defect (Fig. 2IId). At 8 weeks, most defects from TCP-0.1 group achieved complete defect closure by continued formation of new bone around the remaining α-TCP particles as well as in place of resorbed α-TCP particles at the center of defect. There were only a few remaining α-TCP particles demonstrating more diffused borders and reduced in size (Fig. 2IIId).

Table 1. **Percentage of defect closure, bone mineral content (BMC) and bone mineral density (BMD) of the defect at 8 weeks ($n=7$ for each particle-filled group and $n=6$ for control group)**

Experimental groups	Defect closure (%)	BMC (mg)	BMD (mg/cm^2)
Control	41.67 ± 10.78	21.35 ± 0.89	66.05 ± 1.99
TCP-0	74.29 ± 9.48	24.74 ± 1.15	74.97 ± 3.51
TCP-0.01	74.29 ± 6.4	24.71 ± 1.05	74.94 ± 3.17
TCP-0.1	97.86 ± 1.49	29.07 ± 1.11	88.07 ± 3.35
TCP-0.25	82.14 ± 5.55	25.74 ± 1.05	78.01 ± 3.16
TCP-0.5	63.57 ± 9.3	25.49 ± 0.61	77.26 ± 1.84

†$P<0.01$,
*$P<0.05$.
Values are shown as mean ± SEM.
ANOVA percentage of defect closure ($F_{5,35}=5.724$, $P=0.001$), BMC ($F_{5,35}=5.82$, $P=0.001$), BMD ($F_{5,35}=5.483$, $P=0.001$).

TCP-0.25 and TCP-0.5 groups

At 2 weeks, only a scanty amount of new bone was observed at the defect margins (Fig. 2Ie and f). More bone formation became evident at 4 and 8 weeks at the margins without achieving complete defect closure (Figs 2IIe and f and 3IIIe and f).

Radiographic bone volume, defect closure, BMC and BMD

Figure 3 shows the mean bone volumes measured in the micro-CT images at 2, 4 and 8 weeks. The TCP-0.1 group yielded significantly higher bone volumes than untreated control group at all time points (249%, 227% and 266% at 2, 4 and 8 weeks, respectively). At 2 and 8 weeks, the TCP-0.1 group showed significantly higher bone volume than all other groups.

Table 1 demonstrates the percentage of defect closure, BMC and BMD, which were all evaluated at 8 weeks. The percentage of defect closure was significantly higher in TCP-0.1 group than control and TCP-0.5 groups. Moreover, the BMC and BMD values were also significantly higher in TCP-0.1 group than control, TCP-0 and TCP-0.01 groups. TCP-0.25 group also showed higher percentage of defect closure and BMC than control group.

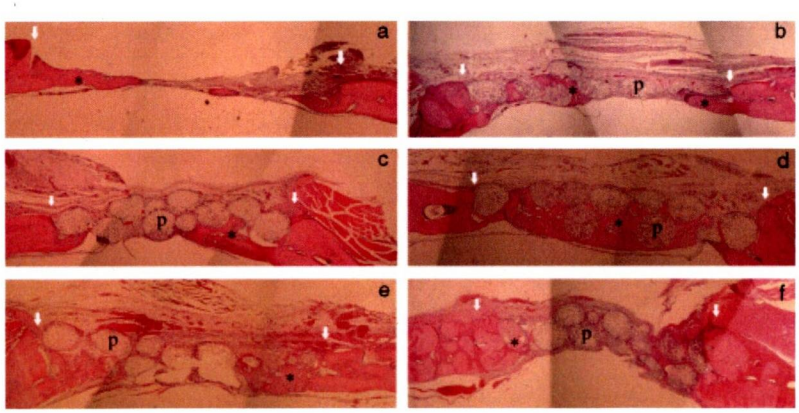

Fig. 4. Photomicrographs of the calvarial defects at 2 weeks representing (a) control, (b) TCP-0, (c) TCP-0.01, (d) TCP-0.1, (e) TCP-0.25 and (f) TCP-0.5 groups. Arrows denote original defect margins. *Newly formed bone; P the α-TCP particle. (Hematoxylin and eosin stain, original magnification × 4).TCP, tricalcium phosphate.

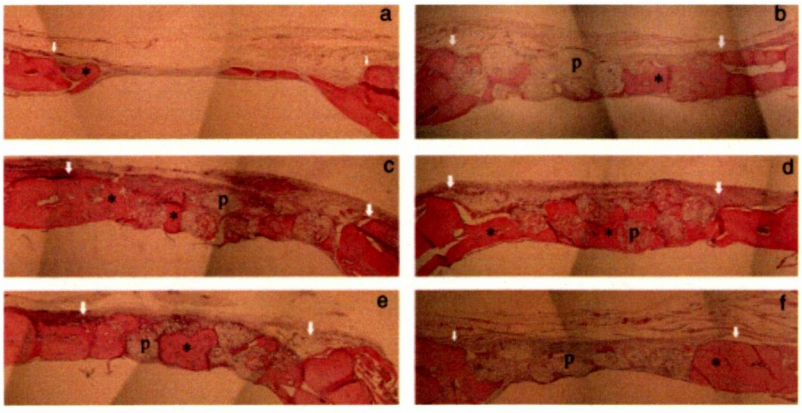

Fig. 5. Photomicrographs of the calvarial defects at 4 weeks representing (a) control, (b) TCP-0, (c) TCP-0.01, (d) TCP-0.1, (e) TCP-0.25 and (f) TCP-0.5 groups. Arrows denote original defect margins. *Newly formed bone; P the α-TCP particle. (Hematoxylin and eosin stain, original magnification × 4).

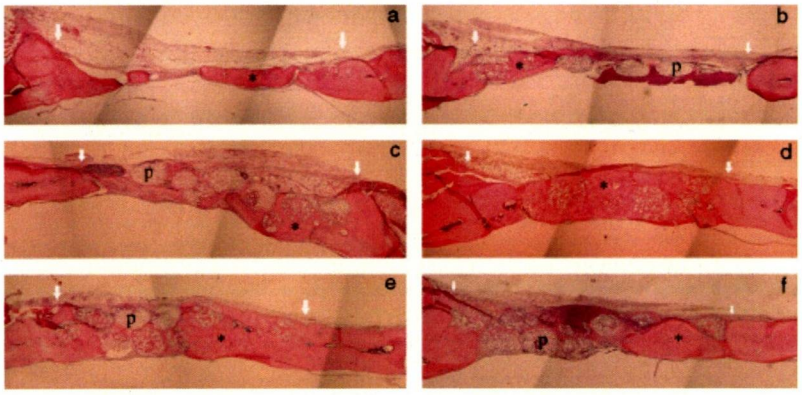

Fig. 6. Photomicrographs of the calvarial defects at 8 weeks representing (a) control, (b) TCP-0, (c) TCP-0.01, (d) TCP-0.1, (e) TCP-0.25 and (f) TCP-0.5 groups. Arrows denote original defect margins. *Newly formed bone; P the α-TCP particle. (Hematoxylin and eosin stain, original magnification × 4). TCP, tricalcium phosphate.

Histological observation

Control group

At 2 and 4 weeks, only a thin layer of new bone was seen at the defect margins. The central portion of defect was filled with compressed fibrous connective tissue (Figs 4a and 5a). More new bone was formed towards the center in some defects at 8 weeks (Fig. 6a).

TCP-0 and TCP-0.01 groups

At 2 weeks, only a few areas of newly formed bone were seen at the defect margins and between some adjacent α-TCP particles in TCP-0 group. Each particle demonstrated many spaces inside it forming a reticulate structure. Only a few inflammatory cells were noted generally in the soft tissue (Fig. 4b and c). The areas of new bone became increased at 4 weeks (Fig. 5b and c). Although new bone formation appeared to continue from the defect margins at 8 weeks, both groups still revealed many remaining α-TCP particles (Fig. 6b and c).

TCP-0.1 group

As early as 2 weeks, there were many areas of new bone in between the α-TCP particles in the TCP-0.1 group, characterized by irregular trabeculae of immature bone and osteoid rimmed by osteoblasts. The new bone seemed to be formed abundantly especially near the dura mater surface all over the defect area as well as from the defect margins. Numerous blood vessels were also associated with the newly formed bone. Active osteoblasts lined around the surface of the α-TCP particles and bone matrix appeared to be deposited inside some particles located near the bottom of the defect. At the defect borders, bone had bridged the gap between the defect border and the inserted α-TCP particles. Only a few inflammatory cells were observed in the soft tissue covering the defect (Fig. 4d). At 4 weeks, more advanced bone formation was seen at the center of defects. Moreover, bone matrix appeared to be deposited inside all α-TCP particles in the defect (Fig. 5d). At 8 weeks, most of the defects showed a complete bridging of new bone across the defect by continuous regeneration of bone at the center. New bone was also observed inside the remaining α-TCP particles. Thus, the latter appeared to be partially obliterated by bone (Fig. 6d).

TCP-0.25 and TCP-0.5 groups

At 2 weeks, only a few areas of new bone were seen at the defect margins. There were many inflammatory cells and fibroblasts in the soft tissue covering the defect and also in between some α-TCP particles, which were located close to the soft tissue. Some inflammatory cells infiltrated inside the α-TCP particles. Many collagen fibers filled the space in between the α-TCP particles. The inflammatory cell infiltration was more prominent and extensive in TCP-0.5 group (Fig. 4e and f). At 4 weeks, the inflammatory cells were markedly reduced and more new bone was formed at the margin as well as in some areas at the center of the defect in TCP-0.25 group (Fig. 5e). In TCP-0.5 group, however, the amount of new bone did not increase showing many α-TCP particles, which were still invaded by fibroblasts and some inflammatory cells (Fig. 5f). At 8 weeks, a considerable amount of bone was formed in the TCP-0.25 group, but there was no complete bridging of the defect with some remaining particles at the center (Fig. 6e). More bone was formed in TCP-0.5 group at this time point compared with that of 4 weeks; however, the areas of remaining α-TCP particles still predominated the defect (Fig. 6f).

MAR

MAR values were shown in Fig. 7. Consistent with the higher bone volume in TCP-0.1 group, the MAR in this group was significantly higher than those of all other groups at 4 weeks. At 8 weeks, however, there was no statistically significant difference between TCP-0.1 and TCP-0.25 groups whereas other groups (TCP-0, TCP-0.01 and TCP-0.5) still showed significantly lower MARs than that of TCP-

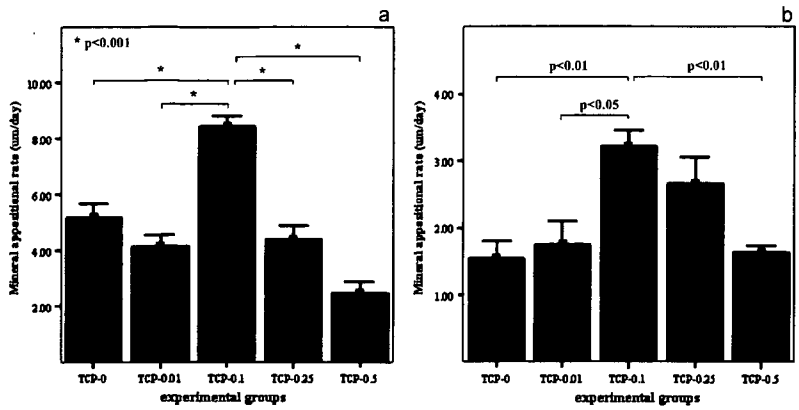

Fig. 7. Mineral apposition rates at (a) 4 weeks and (b) 8 weeks. Bars and error bars represent means and SEM, respectively. $n = 4$ for each group at each time point. ($F_{4,15} = 6.978$, $P = 0.002$).

0.1 group. Relatively higher apposition rate in the TCP-0.25 group at 8 weeks was in line with the increasing bone volume in this group at 8 weeks. In all groups, MARs decreased at 8 weeks compared with those at 4 weeks (Fig. 7a and b).

Discussion

Bone regeneration requires three essential components: firstly, signaling molecule; secondly, scaffold which acts as osteoconductive surface to support osteoblastic bone formation; and thirdly, cells responsible for bone formation. Our strategy is *in situ* tissue regeneration approach in which new tissue formation is induced by specific scaffolds with external stimuli that are used to stimulate body's own cells and promote local tissue repair. We applied different doses of simvastatin combined with osteoconductive α-TCP particles in rat calvarial defects and showed that 0.1 mg simvastatin induced maximum bone regeneration.

Simvastatin is one of the commonly prescribed cholesterol lowering drugs and it has been shown to upregulate BMP-2 and VEGF gene expression in osteoblasts (Mundy et al. 1999; Sugiyama et al. 2000; Garrett et al. 2001; Ohnaka et al. 2001; Maeda et al. 2001, 2003; Ghosh-Choudhury et al. 2007). Administration of statins either systemically or locally has been shown to promote bone growth and/or regeneration (Skoglund et al. 2002; Thylin et al. 2002; Wong & Rabie 2003; Knoch et al. 2005; Sato et al. 2005; Stein et al. 2005; Wong & Rabie 2005a, 2005b; Bradley et al. 2007; Garrett et al. 2007; Nyan et al. 2007; Ozec et al. 2007; Sugiyama et al. 2007). Simvastatin was chosen as the statin to be tested in our study because *in vitro* studies have shown it to be one of the most potent statins in stimulating bone growth (Garrett et al. 2001) and other *in vivo* studies have confirmed its bone-promotive effect.

Although anti-inflammatory effects of statins have been reported (Weitz-Schmidt 2002), high-dose simvastatin induces inflammation around the site of local application. It has been shown that local simvastatin application at 2.2 mg causes inflammation and scabbing of the skin overlying the murine calvaria (Thylin et al. 2002). Stein et al. (2005) applied simvastatin in methyl cellulose gel in a polylactic acid membrane locally on rat mandible at different doses and found that by lowering the simvastatin dose, the signs of inflammation can be reduced and they concluded that 0.5 mg simvastatin is the optimal dose for single local application. In our previous study, 1 mg simvastatin combined with calcium sulfate caused substantial bone regeneration in rat calvarial defects; however, with a considerable soft-tissue inflammation and scabbing of the skin overlying the calvaria (Nyan et al. 2007). Thus, the local effects of simvastatin would be dose- and carrier-dependent. We speculate that a carrier degrading rapidly during the early phase of bone healing would not be desirable for bone regeneration with simvastatin.

Calcium phosphate materials have been shown to be osteoconductive and highly biocompatible (LeGeros 2002) and these materials have been successfully applied as carriers for antibiotics and growth factors such as BMPs (Downes et al. 1991; Guicheux et al. 1998; Blom et al. 2000; Laffargue et al. 2000; Yan et al. 2004; Ginebra et al. 2006; Saito et al. 2006). Among the different calcium phosphate materials, we used α-TCP particles in this study because previous studies have confirmed the role of α-TCP particles as bone-rebuilding material by gradual biodegradation and formation of bone around them (Wiltfang et al. 2002; Kihara et al. 2006). α-TCP is also reported to be able to induce efficient growth of bone cells, and the production of an environment that stimulates osteogenesis *in vitro* (Mayr-Wohlfart et al. 2001; Ehara et al. 2003).

We used rat bilateral calvarial defect model to test our hypothesis, as it is a convenient model for the study of bone-regenerative materials because of its lack of fixation requirements. Experimental models with very young animals are considered unsatisfactory to evaluate osteopromotive materials. The animals used in this study were at adult stage (16 weeks); therefore, increased bone regeneration attributed to growth is not expected.

In our experiment, maximum bone regeneration was consistently observed in the defects applied with the combination of 0.1 mg simvastatin and α-TCP. It is likely to be a result of maximum stimulation of osteoblasts by locally released simvastatin to promote production of BMP-2 and VEGF. In the histological sections of the 2-week samples, many active osteoblasts were observed bordering around the surface of α-TCP particles and depositing bone matrix actively. Osteoblasts originate from osteoprogenitor cells in the bone marrow stroma termed BMSCs or mesenchymal stem cells, and *in vitro* studies have shown that simvastatin promotes osteoblastic differentiation in the human BMSCs and enhances the mineralization of the matrix by the osteoblasts (Song et al. 2003; Baek et al. 2005). We also observed significantly increased MARs in this group suggesting the increased activity of individual osteoblasts.

Stein et al. (2005) demonstrated that 0.1 mg simvastatin clearly showed only a minimal inflammation in terms of swelling and infiltrated area, but little bone growth than the control. The results of our study

are consistent with their observation except the finding that 0.1 mg simvastatin induced the significantly highest bone formation in our study. This difference may be due to the experimental model and simvastatin carrier. They applied simvastatin on the periosteum of intact mandible whereas we applied it in the bone defect. As simvastatin carrier, they used methyl cellulose gel whereas we used α-TCP particles that might be expected releasing the drug efficiently in the bone defect.

Studies on release of proteins from calcium phosphate materials reported a biphasic manner of release; an initial rapid release followed by a gradual long-lasting one (Downes et al. 1991; Guicheux et al. 1998; Blom et al. 2000; Laffargue et al. 2000; Ziegler et al. 2002). It is also likely that a burst initial dose of adsorbed simvastatin was released by α-TCP in early phase of healing in our experiment. Such a release of simvastatin may be advantageous in TCP-0.1 group for providing an optimal dose of the drug that could stimulate local responding cells to express BMP-2 without eliciting an inflammatory reaction. Bone regeneration was apparent in this group since the earliest observation period of 2 weeks. Furthermore, significantly higher values of bone volume at later time points in TCP-0.1 group suggested a maximum stimulation of the local cells by simvastatin. Possibly, sustained release of simvastatin from the gradually degrading α-TCP particles might have provided continued exposure of local osteoblasts to simvastatin resulting in the upregulation of BMP-2 and subsequent stimulation of migrated mesenchymal cells to osteoblastic differentiation. Interestingly, the regenerated bone at 8 weeks seemed to be self-limited by remodeling so that the normal contour of bone surface was achieved.

Notably, the degradation and disappearance of α-TCP particles was the most evident in TCP-0.1 in which bone formation was the most prominent. In this particular group, it is likely that bone remodeling together with bone formation was remarkably enhanced. As a result, α-TCP particles might be rapidly degraded and exchanged to new bone in this group.

In contrast, the released simvastatin from TCP-0.25 and TCP-0.5 groups seemed to cause exacerbation of the normal inflammatory reaction in local wound environment in the early phase of bone healing. Although inflammation is the initiator of healing, an excessive or aberrant inflammatory response is well recognized as a major contributing factor to delayed healing in both animal and human models (Szpaderska & DiPietro 2005; Eming et al. 2007; Menke et al. 2007). Bunn et al. (2005) reported that bone healing was impaired in the fracture model associated with overlying muscle crush injury in which the excess inflammation caused increased production of inflammatory cytokines. In our study, despite the promotion of BMP-2 expression by simvastatin, the excessive inflammation in the higher-dose groups might have induced the production of inflammatory cytokines, excess of which may be deleterious for differentiation and/or subsequent mineralization of osteoblasts. The net result was less new bone formation in these groups compared with TCP-0.1 group, not only in the early phase but also in the later time points. The difference was more obvious in defects grafted with 0.5 mg simvastatin with α-TCP in which more intense and prolonged inflammation had been observed. On the other hand, 0.01 mg simvastatin appeared to be insufficient to stimulate bone healing in this experiment.

In addition to the effects of locally released simvastatin, bioactivity and osteoconductivity of α-TCP particles may also play an important role in the maximum bone regeneration in TCP-0.1 group. It is well established that partial dissolution of calcium phosphate biomaterials causes liberation of calcium and phosphate ions into the microenvironment, which in term promotes bone mineralization and enhances bone formation (LeGeros 2002). As we had reported previously (Kihara et al. 2006), the new bone was formed on the surface of TCP particles and inside the particles in the present study, which further supports the osteoconductivity of α-TCP particles.

The outcome of any type of regenerative procedure is strongly dependent upon the available space under the mucoperiosteal flap (Wikesjo & Selvig 1999). In the present study, the flap collapse in particle-filled defects seemed to be prevented by the use of α-TCP particles as we had observed in the previous study (Kihara et al. 2006). All the particle-filled defects yielded more bone regeneration than empty control defects. This space-maintaining property of α-TCP is advantageous in the bone augmentation procedures.

The empty defects in the negative control group and the defect adjacent to the positive control (α-TCP only) group revealed formation of only a thin layer of new bone along the periphery of defect. Notably, the unfilled empty defects contralateral to those filled with simvastatin–TCP combination showed considerable bone regeneration and healed well (data not shown). This finding suggested a possible paracrine manner of bone formation-stimulating signal from the filled defects with simvastatin–TCP combination.

In conclusion, our study confirmed the bone promoting effect of local simvastatin and determined that 0.1 mg was the optimal dose for the maximum bone regeneration of 5-mm-diameter bone defects in rat calvaria when applied in combination with α-TCP. Further studies are required to validate the effect of this optimal dose of simvastatin with α-TCP combination in different clinical situations.

Acknowledgements: This research was supported by the grant for Center of Excellence Program for Frontier Research on Molecular Destruction and Reconstruction of Tooth and Bone in Tokyo Medical and Dental University and by a Grant (19390513) from the Ministry of Education, Science and Culture, Japan.

References

Baek, K.H., Lee, W.Y., Oh, K.W., Tae, H.J., Lee, J.M., Lee, E.J. & Han, J.H. (2005) The effect of simvastatin on the proliferation and differentiation of human bone marrow stromal cells. *Journal of Korean Medical Science* 20: 438–444.

Blom, E.J., Klein-Nulend, J., Klein, C.P., Kurashina, K., van Waas, M.A. & Burger, E.H. (2000) Transforming growth factor-beta1 incorporated during setting in calcium phosphate cement stimulates bone cell differentiation in vitro. *Journal of Biomedical Materials Research* **50**: 67–74.

Bradley, J.D., Cleverly, D.G., Burns, A.M., Helm, N.B., Schmid, M.J., Marx, D.B., Cullen, D.M. & Reinhardt, R.A. (2007) Cyclooxygenase-2 inhibitor reduces simvastatin-induced bone morphogenic protein-2 and bone formation *in vivo*. *Journal of Periodontal Research* **42**: 267–273.

Bunn, R.J., Burke, G., Connelly, C., Li, G. & Marsh, D. (2005) Inflammation-A double edged sword in high-energy fractures? *Journal of Bone and Joint Surgery – British Volume* **87-B** (Suppl. III): 265–266.

Downes, S., DiSilvio, L., Klein, C.P.A.T. & Kayser, M.V. (1991) Growth hormone loaded bioactive ceramics. *Journal of Materials Science: Materials in Medicine* **2**: 176–180.

Ehara, A., Ogata, K., Imazato, S., Ebisu, S., Nakano, T. & Umakoshi, Y. (2003) Effects of α-TCP and TetCP on MC3T3-E1 proliferation, differentiation and mineralization. *Biomaterials* **24**: 831–836.

Einhorn, T.A. (2003) Clinical applications of recombinant human BMPs: early experience and future development. *Journal of Bone Joint Surgery (Am)* **85** (Suppl. 3): 82–88.

Eming, S.A., Krieg, T. & Davidson, J.M. (2007) Inflammation in wound repair: molecular and cellular mechanisms. *Journal of Investigative Dermatology* **127**: 514–525.

Garrett, I.R., Gutierrez, G. & Mundy, G.R. (2001) Statins and bone formation. *Current Pharmacological Design* **7**: 715–736.

Garrett, I.R., Gutierrez, G.E., Rossini, G., Nyman, J., McCluskey, B., Flores, A. & Mundy, G.R. (2007) Locally delivered lovastatin nanoparticles enhance fracture healing in rats. *Journal of Orthopedic Research* **25**: 1351–1357.

Ghosh-Choudhury, N., Mandal, C.C. & Choudhury, G.G. (2007) Statin-induced Ras activation integrates the phosphatidylinositol 3-kinase signal to Akt and MAPK for bone morphogenetic protein-2 expression in osteoblast differentiation. *Journal of Biological Chemistry* **282**: 4983–4993.

Ginebra, M.P., Traykova, T. & Planell, J.A. (2006) Calcium phosphate cements as bone drug delivery systems: a review. *Journal of Controlled Release* **113**: 102–110.

Guicheux, J., Gauthier, O., Aguado, E., Heymann, D., Pilet, P., Couillaud, S., Faivre, A. & Daculsi, G. (1998) Growth hormone-loaded macroporous calcium phosphate ceramic: *in vitro* biopharmaceutical characterization and preliminary in vivo study. *Journal of Biomedical Materials Research* **40**: 560–566.

Kihara, H., Shiota, M., Yamashita, Y. & Kasugai, S. (2006) Biodegradation process of α-TCP particles and new bone formation in a rabbit cranial defect model. *Journal of Biomedical Materials Research Part B: Applied Biomaterials* **79B**: 284–291.

Knoch, von F., Wedemeyer, C., Heckelei, A., Saxler, G., Hilken, G. & Brankamp, J., et al. (2005) Promotion of bone formation by simvastatin in polyethylene particle-induced osteolysis. *Biomaterials* **26**: 5783–5789.

Laffargue, P., Fialdes, P., Frayssinet, P., Rtaimate, M., Hildebrand, H.F. & Marchandise, X. (2000) Adsorption and release of insulin-like growth factor-I on porous tricalcium phosphate implant. *Journal of Biomedical Materials Research* **49**: 415–421.

LeGeros, R.Z. (2002) Properties of osteoconductive biomaterials: calcium phosphates. *Clinical Orthopaedics and Related Research* **395**: 81–98.

Maeda, T., Kawane, T. & Horiuchi, N. (2003) Statins augment vascular endothelial growth factor expression in osteoblastic cells via inhibition of protein prenylation. *Endocrinology* **144**: 681–692.

Maeda, T., Matsunuma, A., Kawane, T. & Horiuchi, N. (2001) Simvastatin promotes osteoblast differentiation and mineralization in MC3T3-E1 Cells. *Biochemical and Biophysical Research Communications* **280**: 874–877.

Mayr-Wohlfart, U., Fiedler, J., Gunther, K.P., Puhl, W. & Kessler, S. (2001) Proliferation and differentiation rates of a human osteoblast-like cell line (SaOS-2) in contact with different bone substitute materials. *Journal of Biomedical Materials Research* **57**: 132–139.

Menke, N.B., Ward, K.R., Witten, T.M., Bonchev, D.G. & Diegelmann, R.F. (2007) Impaired wound healing. *Clinics in Dermatology* **25**: 19–25.

Mundy, G., Garrett, R., Harris, S., Chan, J., Chen, D., Rossini, G., Boyce, B., Zhao, M. & Gutierrez, G. (1999) Stimulation of bone formation in vitro and in rodents by statins. *Science* **286**: 1946–1949.

Nyan, M., Sato, D., Oda, M., Machida, T., Kobayashi, H., Nakamura, T. & Kasugai, S. (2007) Bone formation with the combination of simvastatin and calcium sulfate in critical-sized rat calvarial defect. *Journal of Pharmacological Science* **104**: 384–386.

Ohnaka, K., Shimoda, S., Nawata, H., Shimokawa, H., Kaibuchi, K., Iwamoto, Y. & Takayanagi, R. (2001) Pitavastatin enhanced BMP-2 and osteocalcin expression by inhibition of Rho-associated kinase in human osteoblasts. *Biochemical and Biophysical Research Communications* **287**: 337–342.

Ozec, I., Kilic, E., Gumus, C. & Goze, F. (2007) Effect of local simvastatin application on mandibular defects. *Journal of Craniofacial Surgery* **18**: 546–550.

Saito, A., Suzuki, Y., Kitamura, M., Ogata, S., Yoshihara, Y., Masuda, S., Ohtsuki, C. & Tanihara, M. (2006) Repair of 20-mm long rabbit radial bone defects using BMP-derived peptide combined with an α-tricalcium phosphate scaffold. *Journal of Biomedical Materials Research* **77A**: 700–706.

Sato, D., Nishimura, K., Ishioka, T., Kondo, H., Kuroda, S. & Kasugai, S. (2005) Local application of simvastatin to rat incisor socket: carrier-dependent effect on bone augmentation. *Journal of Oral Tissue Engineering* **2**: 81–85.

Skoglund, B., Forslund, C. & Aspenberg, P. (2002) Simvastatin improves fracture healing in mice. *Journal of Bone and Mineral Research* **17**: 2004–2008.

Song, C., Guo, Z., Ma, Q., Chen, Z., Liu, Z., Jia, H. & Dang, G. (2003) Simvastatin induces osteoblastic differentiation and inhibits adipocytic differentiation in mouse bone marrow stromal cells. *Biochemical and Biophysical Research Communications* **308**: 458–462.

Stein, D., Lee, Y., Schmid, M.J., Killpack, B., Genrich, M.A., Narayana, N., Mark, D.B., Cullen, D.M. & Reinhardt, R.A. (2005) Local simvastatin effects on mandibular bone growth and inflammation. *Journal of Periodontology* **76**: 1861–1870.

Sugiyama, M., Kodama, T., Konisihi, K., Abe, K., Asami, S. & Oikawa, S. (2000) Compactin and simvastatin, but not pravastatin, induce bone morphogentic-2 in human osteosarcoma cells. *Biochemical Biophysical Research Communications* **271**: 688–692.

Sugiyama, T., Nakagawa, T., Sato, C., Fujii, T., Mine, K., Shimizu, K., Murata, T. & Tagawa, T. (2007) Subcutaneous administration of lactone form of simvastatin stimulates ectopic osteoinduction by rhMBP-2. *Oral Diseases* **13**: 228–233.

Szpaderska, A. & DiPietro, L.A. (2005) Inflammation in surgical wound healing: friend or foe? *Surgery* **137**: 571–573.

Thylin, M.R., McConnell, J.C., Schmid, M.J., Reckling, R.R., Ojha, J., Bhattacharyya, I., Marx, D.V. & Reinhardt, R.A. (2002) Effects of statin gels on murine calvarial bone. *Journal of Periodontology* **73**: 1141–1148.

Weitz-Schmidt, G. (2002) Statins as anti-inflammatory agents. *Trends in Pharmacological Sciences* **23**: 482–487.

Wikesjo, U.M.E. & Selvig, K.A. (1999) Periodontal wound healing and regeneration. *Periodontology 2000* **19**: 21–39.

Wiltfang, J., Merten, H.A., Schlegel, K.A., Schultze-Mosgau, S., Kloss, F.R., Rupprecht, S. & Kessler, P. (2002) Degradation characteristics of α and β tri-calcium-phosphate (TCP) in minipigs. *Journal of Biomedical Materials Research* **63**: 115–121.

Wong, R.W.K. & Rabie, A.B.M. (2003) Statin collagen grafts used to repair bone defects in the parietal bone of rabbits. *British Journal of Oral and Maxillofacial Surgery* **41**: 244–248.

Wong, R.W.K. & Rabie, A.B.M. (2005a) Histologic and ultrastructural study on statin graft in rabbit skulls. *Journal of Oral and Maxillofacial Surgery* **63**: 1515–1521.

Wong, R.W.K. & Rabie, A.B.M. (2005b) Early healing pattern of statin-induced osteogenesis. *British Journal of Oral and Maxillofacial Surgery* **43**: 46–50.

Yan, W.Z., Zhou, D.L., Yin, S.Y., Yin, G.F., Gao, L.D. & Zhang, Y. (2004) Osteogenesis capacity of a novel BMP/α-TCP bioactive composite bone cement. *Journal of Wuhan University of Technology – Materials Science* **19**: 30–34.

Ziegler, J., Mayr-Wohlfart, U., Kessler, S., Breitig, D. & Gunther, K.P. (2002) Adsorption and release properties of growth factors from biodegradable implants. *Journal of Biomedical Materials Research* **59**: 422–428.

Effects of Cholesterol-Bearing Pullulan (CHP)-Nanogels in Combination with Prostaglandin E1 on Wound Healing

Hiroshi Kobayashi,[1] Osamu Katakura,[1] Nobuyuki Morimoto,[2] Kazunari Akiyoshi,[2,3] Shohei Kasugai[1,3]

[1] Oral Implantology and Regenerative Dental Medicine, Tokyo Medical and Dental University, Bunkyo-ku, Tokyo 113-8549, Japan

[2] Institute of Biomaterials and Bioengineering, Tokyo Medical and Dental University, Chiyoda-ku, Tokyo 101-0062, Japan

[3] Global Center of Excellence (GCOE) Program, International Research Center for Molecular Science in Tooth and Bone Diseases, Tokyo, Japan

Received 12 February 2008; revised 11 November 2008; accepted 18 November 2008
Published online 16 April 2009 in Wiley InterScience (www.interscience.wiley.com). DOI: 10.1002/jbm.b.31373

Abstract: The cholesterol-bearing pullulan (CHP)-nanogels are able to trap hydrophobic drugs or proteins inside the nanogels, which is potential in application to drug delivery system and tissue engineering. On the other hand, prostaglandin E1 (PGE1) plays important roles in wound healing and PGE1 ointment has been clinically used to treat chronic skin ulcers and wounds. The purpose of this study is to evaluate effects of CHP nanogels in combination with prostaglandin E1 on wound healing in full thickness skin defect model. A square skin defect (1×1 cm^2) of full thickness was created on the dorsal of Wistar rats. The wound was treated with CHP nanogels without PGE1 (CHP group) or CHP nanogels containing with PGE1 (CHP/PGE1 group) or PGE1 ointment (PGE1 ointment group). In both CHP/PGE1 and PGE1 ointment groups, ~6 μg of PGE1 was applied to each wound. In the control group, the wound was untreated. The wound was evaluated in measuring wound area and histologically. In CHP/PGE1 group, the rate of wound size reduction was significantly higher than the ones of other groups. Histologically, CHP/PGE1 promoted neoepithelialization, neovascularization, and wound closure compared to the other treatments. These results suggest that CHP in combination with PGE1 can promote wound healing, which confirms the efficiency of CHP nanogels-based drug delivery system. © 2009 Wiley Periodicals, Inc. J Biomed Mater Res Part B: Appl Biomater 91B: 55–60, 2009

Keywords: drug delivery system; nanogel; cholesterol-bearing pullulan; prostaglandin E1; wound healing

INTRODUCTION

Wound healing in the skin is a complex biological process in which numerous types of cells, cytokines, growth factors, proteases, and extracellular matrix components play roles. Enhanced epidermal healing in a moist wound environment was demonstrated by Winter in 1962.[1] Furthermore, Vogt et al. reported that a moist or wet healing environment resulted in less necrosis and faster and better quality of healing in the formation of newly regenerated epidermis.[2] Thus, a moist environment is known to accelerate wound re-epithelialization. The ideal wound dressing is biocompatible, protecting the wound from bacterial infection, preventing excessive fluid loss and maintaining a moist healing environment.[3] Currently, various materials, such as gelatin, collagen, polyurethane, and polyethylene are clinically used for wound dressing. Although these wound dressing materials are effective, a wound dressing material, which promotes wound healing more effectively, is strongly required because tremendous number of patients suffer from unhealed wounds, which accompany infection in most cases.

Cholesterol-bearing pullulan (CHP) form nanometer-sized hydrogel (nanogel) by self-assembly in water.[4] The CHP nanogels have multihydrophobic domains consisting of several cholesteryl groups in pullulan.[5] Therefore, CHP nanogels can trap hydrophobic drugs and proteins inside the nanogels and the complex has been applied as drug carriers.[6–8] In our previous reports, PGE2 was trapped in CHP nanogels and injected on to the calvarias of mice, which enhanced local bone formation without any visible side effect.[9] In the case of semi dilute condition of CHP nanogels, physically cross-linked hydrogel is obtained.[10] Using this property, we developed paste (hydrogel) type CHP-nanogels/PGE1 complex.

The biological functions of prostaglandins (PGs) have been widely studied. Prostaglandin E1 (PGE1) is a metabo-

Correspondence to: H. Kobayashi (e-mail: hiro.irm@tmd.ac.jp)

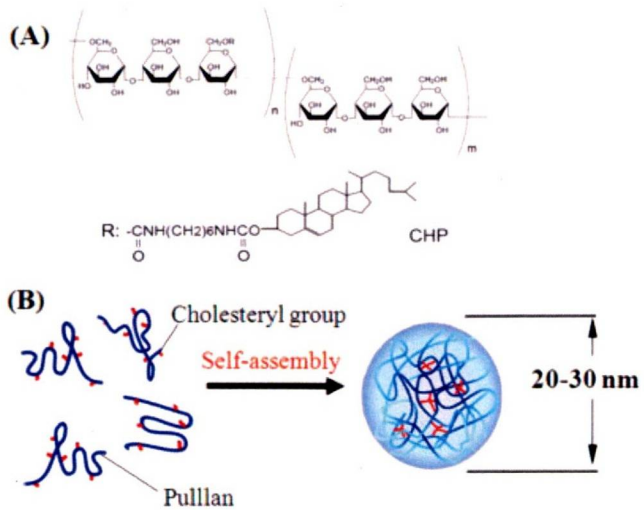

Figure 1. Self-assembly of CHP nanogel and crosslinking based nanogel spheres. (A) Chemical structure of CHP. (B) Formation of nanogel by self-assembly of CHP. [Color figure can be viewed in the online issue, which is available at www.interscience.wiley.com.]

lite of the polyunsaturated dihomogamma-linoleic acid. PGE1 exerts vasodilation and anti-platelet aggregation and it also promotes proliferation of both keratinocytes and fibroblasts.[11] Thus, it has been clinically used to treat burn wounds and various vascular disorders, especially arterial occlusive ischemia. It has been reported that topical application of PGE1 ointment to chronic skin ulcers is effective.[12,13] We speculated that CHP nanogels would be useful as PGE1 carrier for wound treatment. The purpose of this study was to evaluate the effects of CHP nanogels containing prostaglandin E1 *in vivo* full thickness skin defect model.

MATERIALS AND METHODS

Pullulan was substituted with 1.1 cholesterol moieties per 100 anhydrous glucoside units (Figure 1). Cholesterol-bearing pullulan (CHP) was synthesized as previously reported.[4,6–8]

Preparation of CHP Nanogels Containing PGE1

First, CHP nanogels suspension in PBS (pH 7.5, 40 mg/mL) was prepared. PGE1 (Wako Pure Chemical Industries, Ltd. Osaka, Japan) was added directly to the CHP nanogels suspension and mixed by stirring in the dark at room temperature overnight. The final concentration of CHP/PGE1 was 30 μg/mL. The CHP nanogels/PGE1 complex was obtained as paste and it was stored at 4°C.

Experimental Animals

Forty male Wistar rats (7-weeks old; Sankyo Labo Service Corporation; Tokyo, Japan) were used. Each rat was individually kept in a separate cage to avoid an additional wound by the other rats. They were given free access to food and water. The Committee of Animal Experiments of Tokyo Medical and Dental University approved this experiment.

Experimental Model

The rats weighing ~260 g were anesthetized with an intramuscular injection of ketamine (2 mg/kg body weight) and xylazine (0.25 mg/kg body weight) before the surgery. The dorsal skin was shaved with electric clippers and disinfected with 70% ethanol. A full-thickness square surgical wound, 1×1 cm^2 in size, was prepared on the dorsal skin of each rat. The animals were divided into four groups: the first group was untreated (control group), the second group was applied with CHP nanogels only (CHP group), the third group was applied with CHP nanogels containing PGE1 (CHP/PGE1 group), the fourth group was applied with PGE1 ointment (Ono Pharmaceutical Co. Ltd., Osaka, Japan) (PGE1 ointment group). In both CHP/PGE1 and PGE1 ointment groups, 6 μg of PGE1 was approximately applied to each wound. Then, all wounds including the ones in the control group were covered with polyurethane film (Cathereep®, Nichiban Co. Ltd., Tokyo, Japan), over which sterile gauze was layered, and all layers were fixed with elastic adhesive bandage (Elastpore®, Nichiban Co. Ltd., Tokyo, Japan) and sutures. This wound coverage was schematically presented in Figure 2. The above applications to the wounds were performed at the time of wound creation. For the following wound reduction measurement and histological evaluation, the dressing material of each rat was not removed until the time point of observation. However, exceptionally, for taking time-sequential photographic images from one animal of each group, the dressing material was temporally removed and immediately returned back after taking a photo. It is likely that this procedure did not

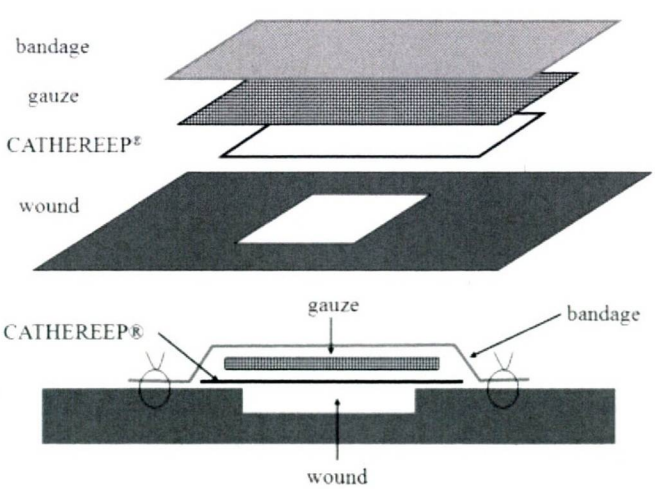

Figure 2. Schematic figure of wound dressing layers in this study.

affect wound healing extensively because the damage of the wound bed was not visually observed during this procedure.

During the experiment, animals were kept in separate cages. The wound together with a ruler was photographed to measure the wound area on day 0, 5, 7, 10, and 14 days after the surgery. In the wound reduction measurements, the photographs were firstly taken and the measurements in the unlabelled photographs were performed. The wound area was measured with an image analysis software (Scion Image). Wound size reduction was calculated by the following numerical formulas:

Wound size reduction (%) = (the original wound area − the wound area on day 5, 7, 10, and 14 day after the surgery) × 100/the original wound area.

Histology

The animals were sacrificed under chloroform anesthesia at 1 and 2 weeks after the surgery. The wounds and their surrounding tissue were excised and then fixed in 10% neutralized-formalin solution. The specimens were dehydrated in ethanol, embedded in paraffin wax and sectioned. The sections were stained with hematoxylin and eosin. For wound re-epithelialization measurement, the photographs were first taken and the measurements in the unlabelled photographs were performed. Percentage of wound re-epithelialization was determined by histomorphometrical analysis. The length of newly generated epithelium across the surface of the wound was determined as the sum of the new epidermis growing from the right and left margins of the wound. This length was expressed as a percentage of initial entire wound length.

Rate of re-epithelialization (%) = (the original wound length − the length of unepithelialized tissues on day 7 and 14 after the surgery) × 100/the original wound length.

Statistical Analyses

All data were presented as the mean ± standard error of mean (SEM). Differences between the groups were examined with Tukey for a multiple comparison test. A value of $p < 0.05$ was considered to be statistically significant.

RESULTS

The images of the wounds of all groups at 0, 7, and 14 days were presented in Figure 3. We measured the wound area at 0, 5, 7, 10, and 14 days and calculated wound size reduction. Figure 4 shows the wound size reduction of all groups at 5, 7, 10, and 14 days. Obviously, wound size reduction of CHP/PGE1 group was superior to the ones of other three groups at every time point. Furthermore, wound size reduction of the CHP group was higher than that of the control groups at all four time points. Interestingly, wound size reduction of CHP group was higher than that of the PGE1 ointment group at 5 and 14 days.

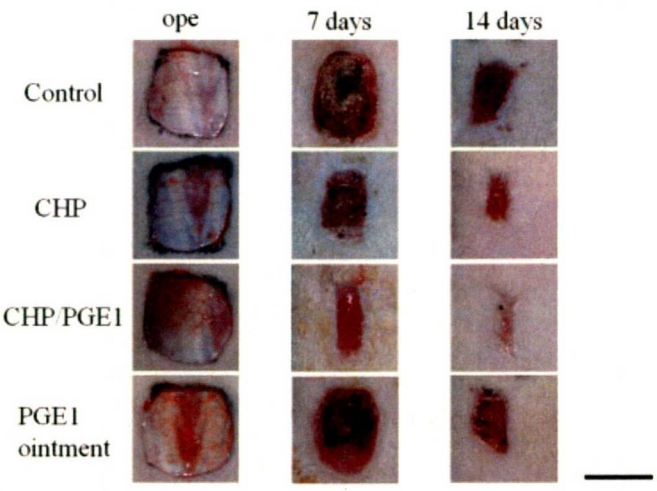

Figure 3. Photographic result of wounds covered with CHP, CHP/PGE1, and PGE1 ointment compared with untreated (control). Black line: 10 mm. [Color figure can be viewed in the online issue, which is available at www.interscience.wiley.com.]

Figure 5 shows the rate of wound re-epithelialization of all groups at 7 and 14 days. At 7 days, the rate of re-epithelialization of CHP/PGE1 group was higher than those of other three groups. At 14 days, the rate of re-epithelialization of CHP/PGE1 group was significantly higher than those of the control and PGE1 ointment groups. At 14 days in CHP group re-epithelialization was more prominent than those of the control and PGE1 ointment groups.

To evaluate the quality of the regenerated tissues, we performed hematoxylin-eosin (H-E) staining of the histological sections. Figure 6 shows the histological images of the wound tissues of all groups at 7 days. In the control group [Figure 6(A)], approximately one-third of the wound was covered with epithelium; however, the other wound surface was covered by necrotic tissue under which numerous neutrophils and macrophages were observed. The granulation tissue, which included numerous inflammatory cells, was evident in the dermis, and a scab was formed over the wound. In the CHP group [Figure 6(B)], epithelium covered approximately a half of the wound and numerous inflammatory cells were similarly observed in dermis, where more capillaries were observed compared to the control group. In the CHP/PGE1 group [Figure 6(C)], the neoepithelium from the edge of the wound was much longer than that of the other groups. In the dermis, there were fewer neutrophils and more capillaries than the control and PGE1 ointment groups. In the PGE1 ointment group [Figure 6(D)], approximately two-fifth of the wound was covered with new epithelium and numerous inflammatory cells were seen in the dermis.

Figure 7 shows the histological images of the wound tissues of all groups at 14 days. In the control group [Figure 7(A)], the wound was not completely covered with epithelium and inflammatory cells still existed in the center of the wound. In the CHP group [Figure 7(B)], the wound was almost completely covered with epithelium and there

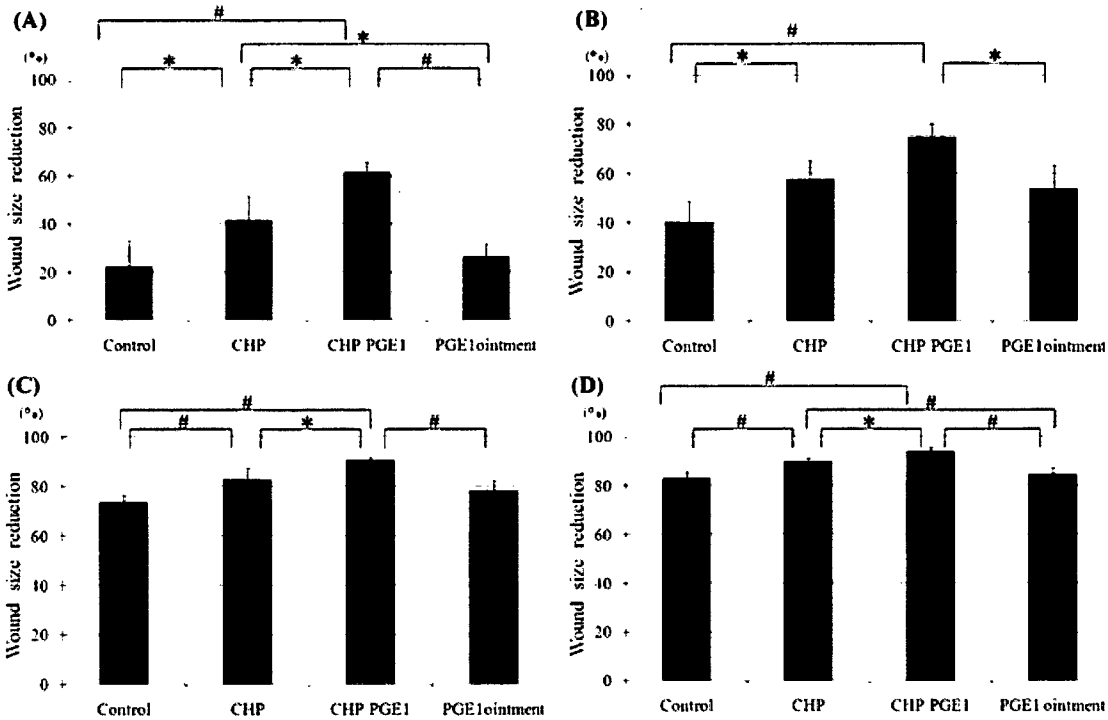

Figure 4. The rate of wound size reduction was calculated at (A) 5 days, (B) 7 days, (C) 10 days, and (D) 14 days. Data are presented as mean ± SEM. $^{\#}p < 0.01$, $^{*}p < 0.05$.

were a few inflammatory cells in the dermis. In the CHP/PGE1 group [Figure 7(C)], skin defect was completely regenerated and covered with new mature epithelium. Inflammatory cells were almost absent. In this group, the epidermal rete pegs were well developed and mature collagen was also present in the dermis. The skin appendage was regenerated. In the PGE1 ointment group [Figure 7(D)], the wound was not completely covered with epithelium and inflammatory cells were still seen in the dermis.

DISCUSSION

The ideal wound dressing should have the following properties: providing a moisturized wound-healing environment, being removable without additional trauma to the wound, protecting the wound from bacterial infection, controlling permeability of oxygen and carbon dioxide, being biocompatible, absorbing wound exudates, and finally promoting tissue reconstruction processes.[14] As wound dressing materials synthetic materials, such as polyurethane,[15–17] polyvinyl alcohol,[18]

polyhydroxyethylmethacrylate,[19] and copolymers,[20] as well as biological materials such as bovine collagen,[21–23] chitin,[24] and alginate[25–27] have been investigated. Compared with these materials, the uniqueness of CHP nanogels is to trap hydrophobic molecules including proteins and nucleic acids. Therefore, this material has been used as polymeric nanocarriers in cancer chemotherapy for protein delivery and for artificial vaccine.[6–8] We speculate that the character of CHP nanogels would also be ideal as a drug-carrier to stimulate wound healing. Interestingly, in this study CHP nanogels application alone accelerated the wound size reduction and epithelialization compared with not only untreatment (control) but also PGE1 ointment treatment, suggesting that CHP nanogels are effective for wound healing.

There would be several reasons for the favorable effects of CHP nanogels in wound healing. Our previous studies have demonstrated high biocompatibility of CHP nanogels,[9] which is one of the required properties for wound dressing. Since CHP nanogels contain more than 90% of water,[5] the water in the gels would be exchanged for wound exudates and keep the wound in wet condition continuously. Wound exudates, which are produced in the process of wound healing, keep the wound in a moist environment and smoothen the migration of the epidermal cells. Moreover, wound exudates contain various growth factors, such as epidermal growth factor, basic fibroblast growth factor, and platelet-derived growth factor, which favorably stimulate wound healing. Thus, it is likely that CHP nanogels trap wound exudates together with various growth factors, which will gradually release from the gels, and that the gels also keep the wound in the moist environment.

PGE1 stimulates the proliferation and cytokine production of epidermal keratinocytes and dermal fibroblasts and it also dilates blood vessels improving peripheral circulation.[11] Thus, it has been expected that when PGE1 is

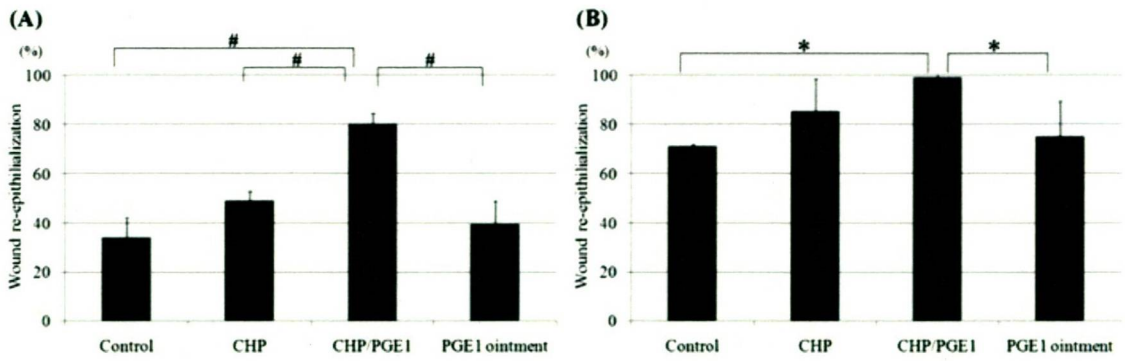

Figure 5. The rate of wound re-epithilialization was calculated at (A) 7 days and (B) 14 days. Data are presented as mean ± SEM. $^{\#}p < 0.01$, $^{*}p < 0.05$.

applied to the wound, PGE1 will directly act on keratinocytes, fibroblasts, and blood vessel cells consequently promoting wound healing. PGE1 ointment has been clinically used to treat skin ulcers and wounds; however, two time applications per day are recommended in the clinical use. In this study, when CHP/PGE1 was applied once to the wound after the wound preparation, the wound was completely covered with new epithelium and inflammatory cells were very few at 14 days. The healing of the wound was extremely well in CHP/PGE1 group compared with the other groups including PGE1 ointment group. The pharmacodynamic characteristics of PGE1 are its poor stability and very brief half-life of about 30 s because PGE1 is promptly oxidized and inactivated.[28] It is likely that CHP nanogels could trap PGE1 inside and protect PGE1 from oxidation and gradually release PGE1 for a prolonged period.

This study is the first report of the CHP nanogels application for wound healing. The present experimental results suggest that CHP nanogels in combination with PGE1 can promote wound healing, which confirms the efficiency of CHP nanogels-based drug delivery system. Using CHP nanogels as PGE1 carrier in the near future, we will be able to decrease the application frequency of PGE1 to the wounds, which is beneficial to both patients and nursing staff.

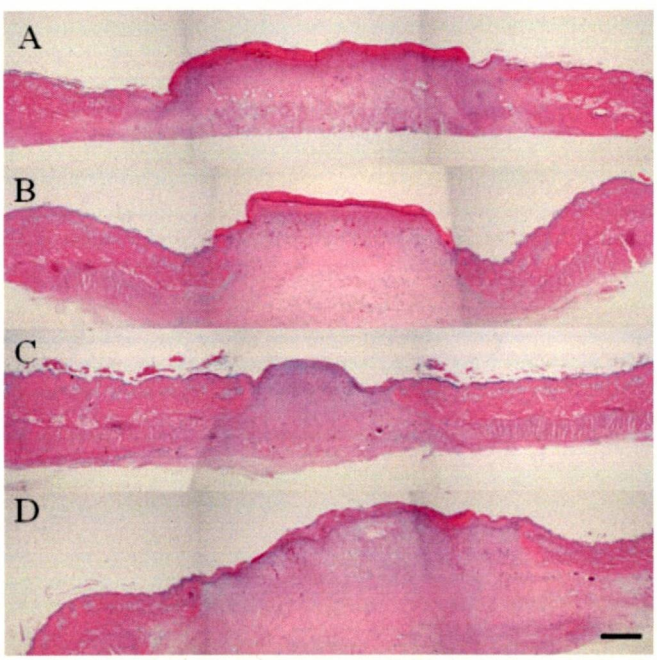

Figure 6. Histological examination of wound tissue stained with hematoxylin and eosin at 7 days: (A) control group; (B) CHP group; (C) CHP/PGE1 group; (D) PGE1 ointment group. Black line: 1 mm. [Color figure can be viewed in the online issue, which is available at www.interscience.wiley.com.]

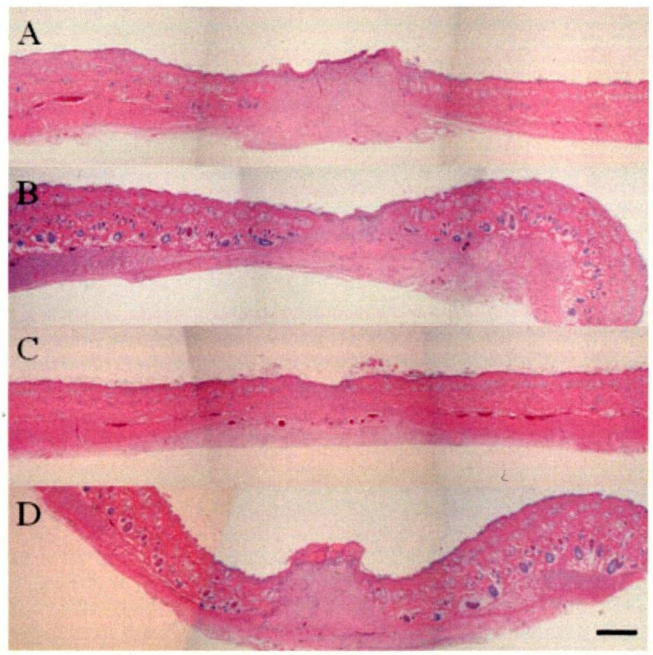

Figure 7. Histological examination of wound tissue stained with hematoxylin and eosin at 14 days: (A) control group; (B) CHP group; (C) CHP/PGE1 group; (D) PGE1 ointment group. Black line: 1 mm. [Color figure can be viewed in the online issue, which is available at www.interscience.wiley.com.]

CONCLUSION

CHP-nanogels are effective for the controlled release of PGE1 and create a moist environment. CHP nanogels in combination with PGE1 can promote wound healing. The clinical application of CHP/PGE1 to full-thickness dermal defect would be promising.

The authors greatly appreciate Dr. M. Suzuki, a technician of our laboratory, for assistance and proper technical advises.

REFERENCES

1. Winter G. Formation of the scab and the rate of epithelization of superficial wounds in the skin of the young domestic pig. Nature 1962;193:293–294.
2. Vogt P, Andree C, Breuing K, Liu P, Slama J, Helo G, Eriksson E. Dry, moist, and wet skin wound repair. Ann Plast Surg 1995;34:493–499; discussion 499–500.
3. Purna S, Babu M. Collagen based dressings—A review. Burns 2000;26:54–62.
4. Akiyoshi K, Deguchi S, Tajima H, Nishikawa T, Sunamoto J. Microscopic structure and thermoresponsiveness of a hydrogel nanoparticle by self-assembly of a hydrophobized polysaccharide. Macromolecules 1993;26:3062–3068.
5. Akiyoshi K, Deguchi S, Tajima H, Nishikawa T, Sunamoto J. Microscopic structure and thermoresponsiveness of a hydrogel nanoparticle by self-assembly of a hydrophobized polysaccharide. Macromolecules 1997;30:857–861.
6. Akiyoshi K, Taniguchi I, Fukui H, Sunamoto J. Hydrogel nanoparticle formed by self-assembly of hydrophobized polysaccharide. Stabilization of adriamysin by complexation. Eur J Pharm Biopharm 1996;42:286–290.
7. Akiyoshi K, Kobayashi S, Shichibe S, Mix D, Baudys M, Kim S, Sunamoto J. Self-assembled hydrogel nanoparticle of cholesterol-bearing pullulan as a carrier of protein drugs: Complexation and stabilization of insulin. J Control Release 1998;54:313–320.
8. Ikuta Y, Katayama N, Wang L, Okugawa T, Takahashi Y, Schmitt M, Gu X, Watanabe M, Akiyoshi K, Nakamura H, Kuribayashi K, Sunamoto J, Shiku H. Presentation of a major histocompatibility complex class I-binding peptide by monocyte-derived dendritic cells incorporating hydrophobized polysaccharide-truncated HER2 protein complex: Implications for a polyvalent immuno-cell therapy. Blood 2002;99:3717–3724.
9. Kato N, Hasegawa U, Morimoto N, Saita Y, Nakashima K, Ezura Y, Kurosawa H, Akiyoshi K, Noda M. Nanogel-based delivery system enhances PGE2 effects on bone formation. J Cell Biochem 2007;101:1063–1070.
10. Kuroda K, Fujimoto K, Sunamoto J, Akiyoshi K. Hierarchical self-assembly of hydrophobically modified pullulan in water: Gelation by networks of nanoparticles. Langmuir 2002;18: 3780–3786.
11. Zhang J, Maruyama K, Iwatsuki K, Ono I, Kaneko F. Effects of prostaglandin E1 on human keratinocytes and dermal fibroblasts: a possible mechanism for the healing of skin ulcers. Exp Dermatol 1994;3:164–170.
12. Shirakawa J, Horikawa Y, Yaku H, Takeshi M, Obara H. Combined therapy with prostaglandin E1 ointment and lumbar sympathetic ganglion block on intractable skin ulcers accompanied by Bürger's disease. Masui 1992;41:1000–1003.
13. Morisaki S. Effect of topical application of prostaglandin E1 ointment on chronic skin ulcers and relation between tissue oxygen tension and its clinical efficacy. Skin Res 1993;35: 210–218.
14. Wittaya-areekul S, Prahsarn C. Development and in vitro evaluation of chitosan-polysaccharides composite wound dressings. Int J Pharm 2006;313:123–128.
15. Hinrichs W, Lommen E, Wildevuur C, Feijen J. Fabrication and characterization of an asymmetric polyurethane membrane for use as a wound dressing. J Appl Biomater 1992;3: 287–303.
16. Wright K, Nadire K, Busto P, Tubo R, McPherson J, Wentworth B. Alternative delivery of keratinocytes using a polyurethane membrane and the implications for its use in the treatment of full-thickness burn injury. Burns 1998;24:7–17.
17. Taylor J, Laity P, Hicks J, Wong S, Norris K, Khunkamchoo P, Johnson A, Cameron R. Extent of iron pick-up in deferoxamine-coupled polyurethane materials for therapy of chronic wounds. Biomaterials 2005;26:6024–6033.
18. Suzuki Y, Tanihara M, Nishimura Y, Suzuki K, Kakimaru Y, Shimizu Y. A novel wound dressing with an antibiotic delivery system stimulated by microbial infection. ASAIO J 1997; 43:M854–M857.
19. Dressler D, Barbee W, Sprenger R. The effect of Hydron burn wound dressing on burned rat and rabbit ear wound healing. J Trauma 1980;20:1024–1028.
20. Kim H, Choi E, Oh J, Lee H, Park S, Cho C. Possibility of wound dressing using poly(L-leucine)/poly(ethylene glycol)/poly(L-leucine) triblock copolymer. Biomaterials 2000;21:131–141.
21. Yannas I, Burke J. Design of an artificial skin. I. Basic design principles. J Biomed Mater Res 1980;14:65–81.
22. Yannas I, Burke J, Orgill D, Skrabut E. Wound tissue can utilize a polymeric template to synthesize a functional extension of skin. Science 1982;215:174–176.
23. Boyce S, Christianson D, Hansbrough J. Structure of a collagen-GAG dermal skin substitute optimized for cultured human epidermal keratinocytes. J Biomed Mater Res 1988;22:939–957.
24. Muzzarelli R, Guerrieri M, Goteri G, Muzzarelli C, Armeni T, Ghiselli R, Cornelissen M. The biocompatibility of dibutyryl chitin in the context of wound dressings. Biomaterials 2005;26:5844–5854.
25. Choi Y, Hong S, Lee Y, Song K, Park M, Nam Y. Study on gelatin-containing artificial skin. I. Preparation and characteristics of novel gelatin-alginate sponge. Biomaterials 1999;20: 409–417.
26. Choi Y, Lee S, Hong S, Lee Y, Song K, Park M. Studies on gelatin-based sponges. Part III: A comparative study of cross-linked gelatin/alginate, gelatin/hyaluronate and chitosan/hyaluronate sponges and their application as a wound dressing in full-thickness skin defect of rat. J Mater Sci Mater Med 2001; 12:67–73.
27. Hashimoto T, Suzuki Y, Tanihara M, Kakimaru Y, Suzuki K. Development of alginate wound dressings linked with hybrid peptides derived from laminin and elastin. Biomaterials 2004; 25:1407–1414.
28. Milio G, Minà C, Cospite V, Almasio P, Novo S. Efficacy of the treatment with prostaglandin E-1 in venous ulcers of the lower limbs. J Vasc Surg 2005;42:304–308.

Fully functional bioengineered tooth replacement as an organ replacement therapy

Etsuko Ikeda[a,b,1], Ritsuko Morita[a,c,1], Kazuhisa Nakao[a,c], Kentaro Ishida[a,c], Takashi Nakamura[a,c], Teruko Takano-Yamamoto[d], Miho Ogawa[b], Mitsumasa Mizuno[a,c,d], Shohei Kasugai[e], and Takashi Tsuji[a,b,c,2]

[a]Department of Biological Science and Technology, Faculty of Industrial Science and Technology, and [c]Research Institute for Science and Technology, Tokyo University of Science, Noda, Chiba 278-8510, Japan; [b]Organ Technologies Inc., Tokyo 101-0048, Japan; [d]Division of Orthodontics and Dentofacial Orthopedics, Graduate School of Dentistry, Tohoku University, Sendai, Miyagi 980-8575, Japan; and [e]Oral and Maxillofacial Surgery, Department of Oral Restitution, Division of Oral Health Sciences, Graduate School, Tokyo Medical and Dental University, Tokyo 113-8510, Japan

Edited by Robert Langer, Massachusetts Institute of Technology, Cambridge, MA, and approved June 30, 2009 (received for review March 17, 2009)

Current approaches to the development of regenerative therapies have been influenced by our understanding of embryonic development, stem cell biology, and tissue engineering technology. The ultimate goal of regenerative therapy is to develop fully functioning bioengineered organs which work in cooperation with surrounding tissues to replace organs that were lost or damaged as a result of disease, injury, or aging. Here, we report a successful fully functioning tooth replacement in an adult mouse achieved through the transplantation of bioengineered tooth germ into the alveolar bone in the lost tooth region. We propose this technology as a model for future organ replacement therapies. The bioengineered tooth, which was erupted and occluded, had the correct tooth structure, hardness of mineralized tissues for mastication, and response to noxious stimulations such as mechanical stress and pain in cooperation with other oral and maxillofacial tissues. This study represents a substantial advance and emphasizes the potential for bioengineered organ replacement in future regenerative therapies.

regenerative therapy | transplantation

The current approaches being used to develop future regenerative therapies are influenced by our understanding of embryonic development, stem cell biology, and tissue engineering technology (1–4). One of the more attractive concepts under consideration in regenerative therapy is stem cell transplantation of enriched or purified tissue-derived stem cells (5), or in vitro manipulated embryonic stem (ES) and induced pluripotent stem (iPS) cells (6, 7). This therapy has the potential to restore the partial loss of organ function by replacing hematopoietic stem cells in hematopoietic malignancies (8), neural stem cells in Parkinson's disease (9), mesenchymal stem cells in myocardial infarction (10), and hepatic stem cells in cases of hepatic insufficiency (11).

The ultimate goal of regenerative therapy is to develop fully functioning bioengineered organs that can replace lost or damaged organs following disease, injury, or aging (4, 12–14). The feasibility of this concept has essentially been demonstrated by successful organ transplantations for various injuries and diseases (15). It is expected that bioengineering technology will be developed for the reconstruction of fully functional organs in vitro through the precise arrangement of several different cell species. However, these technologies have not yet achieved 3-dimensional reconstructions of fully functioning organs. To achieve the functional replacement of lost or damaged tissues and organs, the development of 3-dimensional bioengineered tissues comprising a single cell type is now being attempted using biodegradative materials (3), appropriate cell aggregation (16), or uniform cell sheets (17). These are now clinically applied for corneal dysfunction (18), myocardial infarction (19), and hepatic insufficiency (20) using oral mucosal epithelial cells, myocardial cells, and liver cells, respectively, with favorable clinical results.

A concept has also now been proposed to develop a bioengineered organ by reproducing the developmental processes during organogenesis (13, 21, 22). Almost all organs arise from their respective germs through reciprocal interactions between the epithelium and mesenchyme in the developing embryo (23–25). Therefore, it is predicted that a functional bioengineered organ could be produced by reconstituting organ germs between epithelial and mesenchymal cells in vitro, although the existence of organ-inductive stem cells in the adult body has not been fully elucidated yet with the exception of hair follicles (26) and the mammary gland (27). Tooth replacement regenerative therapy, which is also induced by typical reciprocal epithelial, and mesenchymal interactions (25, 28), is thought to be a feasible model system to evaluate the future clinical application of bioengineered organ replacement (13, 21). The strategy to develop a bioengineered third tooth after the loss of deciduous and permanent teeth is to properly reproduce the processes which occur during embryonic development through the reconstitution of a bioengineered tooth germ in vitro (21). We have recently developed a method for creating 3-dimensional bioengineered organ germ, which can be used as an ectodermal organ such as the tooth or whisker follicle (29). Our analyses have provided an effective method for reconstituting this organ germ and raised the possibility of tooth replacement with integrated blood vessels and nerve fibers in an adult oral environment (29). However, it remains to be determined whether a bioengineered tooth can achieve full functionality, including sufficient masticatory performance, biomechanical cooperation with tissues in the oral and maxillofacial regions, and proper responsiveness via sensory receptors to noxious stimulations in the maxillofacial region. There are currently no published reports describing successful replacement with a fully functional bioengineered organ.

In our current study, we describe a fully functioning tooth replacement achieved by transplantation of a bioengineered tooth germ into the alveolar bone of a lost tooth region in an adult mouse. We propose this as a model for future organ replacement therapy. The bioengineered tooth, which was erupted and reached occlusion in the oral environment, had the correct tooth structure, hardness of mineralized tissues for mastication, and responsiveness to experimental orthodontic treatment and noxious stimulation in cooperation with tissues in the oral and maxillofacial regions. Our results thus demonstrate

Author contributions: T.T. designed research; E.I., R.M., and K.N. performed research; E.I., K.N., T.T.-Y., and S.K. contributed new reagents/analytic tools; E.I., R.M., K.N., K.I., T.N., M.O., and M.M. analyzed data; and E.I., R.M., K.N., and T.T. wrote the paper.

The authors declare no conflict of interest.

This article is a PNAS Direct Submission.

Freely available online through the PNAS open access option.

[1]E.I. and R.M. contributed equally to this work.

[2]To whom correspondence should be addressed. E-mail: t-tsuji@rs.noda.tus.ac.jp.

This article contains supporting information online at www.pnas.org/cgi/content/full/0902944106/DCSupplemental.

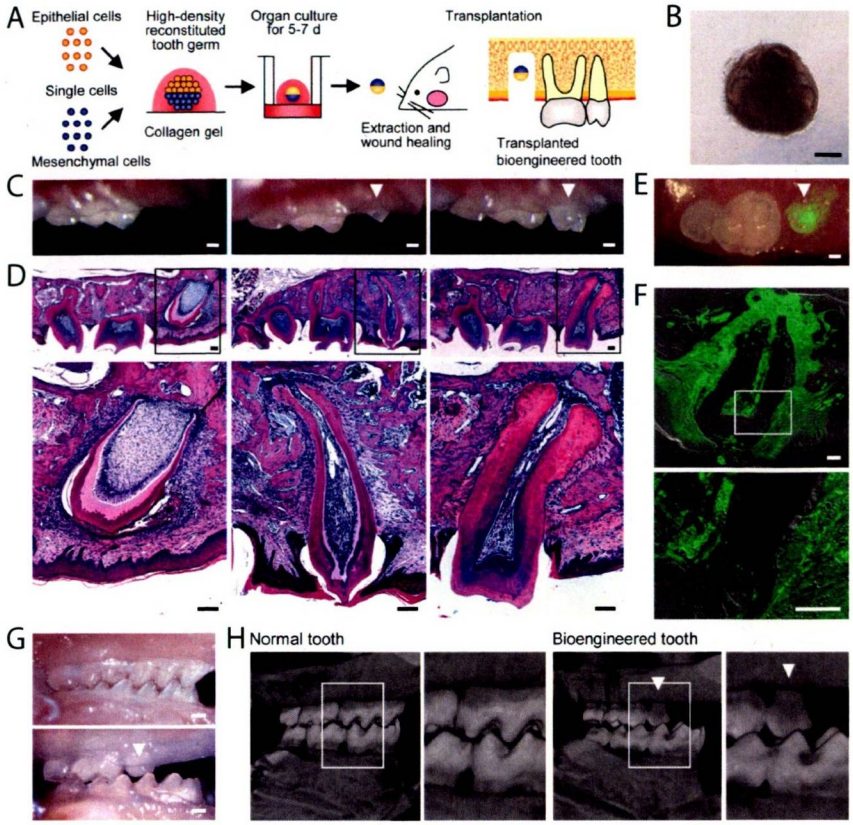

Fig. 1. Eruption and occlusion of a bioengineered tooth. (*A*) Schematic representation of the transplantation technology used for the generation of reconstituted tooth germ. (*B*) Phase contrast image of bioengineered tooth germ on day 5 of an organ culture. (Scale bar, 200 μm.) (*C*) Oral photographs of a bioengineered tooth during eruption and occlusion processes, including before eruption (*Left*), immediately after eruption (*Center*), and full occlusion (*Right*). (Scale bar, 200 μm.) (*D*) Histological analysis of the bioengineered tooth during the eruption and occlusion processes, including before eruption (*Left*), immediately after eruption (*Center*), and full occlusion (*Right*). (Scale bar, 100 μm.) (*E*) Oral photograph of a bioengineered tooth reconstituted using a combination of epithelial cells from normal mice and mesenchymal cells from GFP-transgenic mice (GFP bioengineered tooth). A merged image is shown. (Scale bar, 200 μm.) (*F*) A sectional image of a GFP bioengineered tooth. Fluorescent and DIC images are merged. (Scale bar, 100 μm.) (*G*) Oral photographs showing occlusion of normal (*Upper*) and bioengineered (*Lower*) teeth. (Scale bar, 200 μm.) (*H*) MicroCT images of the occlusion of normal (*Left*) and bioengineered (*Right*) teeth. External (*Left*) and cross section (*Right*) images are shown. The bioengineered tooth is indicated by the arrowhead.

the potential of bioengineered organ replacement for use in future regenerative therapies.

Results

Eruption and Occlusion of a Bioengineered Tooth. We first investigated whether a bioengineered molar tooth germ, which was reconstituted from embryonic day 14.5 (ED14.5) molar tooth germ-derived epithelial and mesenchymal cells by our previously developed organ germ method, could erupt and reach occlusion with an opposing tooth in the mouse adult oral environment (Fig. 1*A*). After 5–7 days in an organ culture, a single bioengineered molar tooth germ, which had developed at the early bell stage of a natural tooth germ and was with a mean length of 534.4 ± 45.6 μm (Fig. 1*B*), was then transplanted with the correct orientation into a properly-sized bony hole in the upper first molar region of the alveolar bone in an 8-week-old adult murine lost tooth transplantation model. In this model, the upper first molar had been extracted, and the resulting wounds had been allowed to heal for 3 weeks (Fig. 1*A* and Fig. S1*A*). The cusp tip of the bioengineered tooth was exposed into the oral cavity at 36.7 ± 5.5 days after transplantation at a frequency of 34/60 (56.6%) (Fig. 1*C Center* and Fig. S1 *B–D Center*). In current transplantation model, the non-erupted explants also occurred at low frequency and were due to the microsurgery for the transplantation, such as transplantation with the reverse direction or the falling off the explants. The vertical dimension of the tooth crown continually increased and the bioengineered tooth finally reached the plane of occlusion with the opposing lower first molar at 49.2 ± 5.5 days after transplantation (Fig. 1*C Right*, and Fig. S1 *B–D Right* and *E*). During the course of eruption and occlusion, the alveolar bone at the bony hole gradually healed in the areas around the bioengineered tooth and the regenerated tooth had sufficient periodontal space between itself and the alveolar bone (Fig. 1*D* and Fig. S1*D*). The bioengineered tooth also formed a correct structure comprising enamel, ameloblast, dentin, odontoblast, dental pulp, alveolar bone, and blood vessels (Fig. 1*D*). It is known that mice have a considerable amount of cellular cementum that increases in thickness both on the sides of the roots and in the interradicular area and forms around the apex of the molar roots (30). The fully occluded bioengineered tooth was also observed to have a large amount of cellular cementum that was equivalent to a normal murine molar tooth (Fig. 1*D* and Fig. S1*A*). The root of the bioengineered tooth was also observed to be surrounded by sufficient periodontal ligaments (PDL) (Fig. 1*D*). Observations of the bioengineered tooth morphology revealed that the crown had plural cusp structure. The lengths and crown widths of the erupted bioengineered teeth were 1,474.4 ± 115.1 and 690.7 ± 177.7 μm, respectively. However, the bioengineered tooth was smaller than the other normal teeth, since at present we cannot regulate the crown width, cusp position, and tooth patterning including anterior/posterior and buccal/lingual structures using in vitro cell manipulation techniques.

We also transplanted green fluorescence protein (GFP)-labeled bioengineered tooth germ, which was reconstituted by normal epithelial cells and the mesenchymal cells from GFP-transgenic mice into non-transgenic mice as described above (29). A GFP-labeled bioengineered tooth was produced and could be observed in the bony hole in the alveolar bone of adult mice (Fig. 1*E* and Fig. S1*F*). GFP-positive mesenchymal cells were also detectable both in the odontoblasts and in the dental pulp and PDL, which differentiate from the dental papilla and dental follicle cells, respectively (Fig. 1*F*). Green fluorescence was also observed in the dentinal tubules of the GFP-positive odontoblasts in the regenerated tooth (Fig. 1*F Lower*).

We next investigated the gene expression profiles of colony-stimulating factor 1 (*Csf1*) and parathyroid hormone receptor (*Pthr1*), which are thought to regulate osteoclastogenesis during

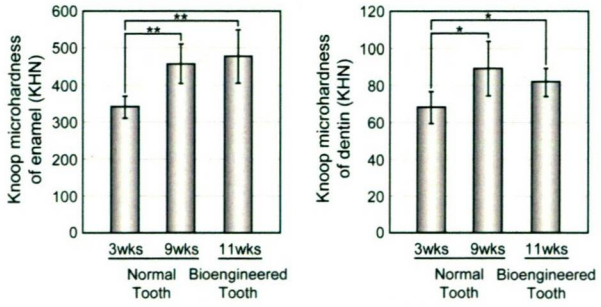

Fig. 2. Assessment of the hardness of the bioengineered tooth. Knoop microhardness values of the enamel (*Left*) and dentin (*Right*) of the bioengineered tooth at 11-weeks post transplantation were compared with those of normal teeth from 3- and 9-week-old mice. Error bars show the standard deviation ($n = 3$). $P < 0.001$ (*) and <0.0001 (**) was regarded as statistically significant (t test).

tooth eruption (31). Those genes were detectable in the eruption pathway and at the boundary surface between the dental follicle of the bioengineered tooth and osseous tissues, as is seen in normal teeth (Fig. S2). These observations suggest that the eruption of the bioengineered tooth germ faithfully reproduced the molecular mechanisms involved in the normal tooth eruption process.

We next analyzed the occlusion established between the bioengineered tooth and the opposing lower teeth. We often observed that the bioengineered tooth moved physiologically before achieving the occlusion during the transplantation experiments. The regenerated tooth achieved normal occlusion in harmony with other teeth in the recipient animal and had opposing cuspal contacts that maintained the proper occlusal vertical dimensions between the opposing arches (Fig. 1 *G* and *H*, and Fig. S1 *B–E*). Following the achievement of occlusion at 49.2 ± 5.5 days after transplantation, there was no excessive increase in the tooth length or perforation of the maxillary sinus by the erupted bioengineered tooth at up to 120 days after transplantation. These results indicated that the bioengineered tooth moved in response to mechanical stress and achieved functional occlusion with the opposing natural tooth.

Masticatory Potential of the Bioengineered Tooth. The masticatory potential of a bioengineered tooth is essential for achieving proper tooth function (32). We thus performed a Knoop hardness test, which is a test for mechanical hardness and is used in particular for very brittle materials or thin sheets. This was an important parameter for evaluating masticatory functions in our bioengineered tooth, including both the dentin and the enamel components. The Knoop hardness of both the enamel and dentin of normal teeth in 3-week-old and 9-week-old mice significantly increases in according to the postnatal period (Fig. 2). These values for enamel and dentin in the normal teeth of 9-week-old adult mice were measured at 447.7 ± 88.9 and 88.4 ± 10.2 Knoop hardness number (KHN), respectively (Fig. 2). The same measurements in the bioengineered tooth were 461.1 ± 83.2 and 81.4 ± 7.53 KHN, respectively (Fig. 2). These findings indicated that the hardness of the bioengineered tooth is in the normal range.

Bioengineered Tooth Response to Mechanical Stress. It has been postulated that regeneration of a fully functional tooth could be achieved by fulfilling critical functions in an adult oral environment such as the cooperation of the bioengineered tooth with the oral and maxillofacial regions through the PDL (31, 33). Histochemical analysis of the PDL of our bioengineered tooth (Fig. 1*D*) showed a positive connection between this tooth and the

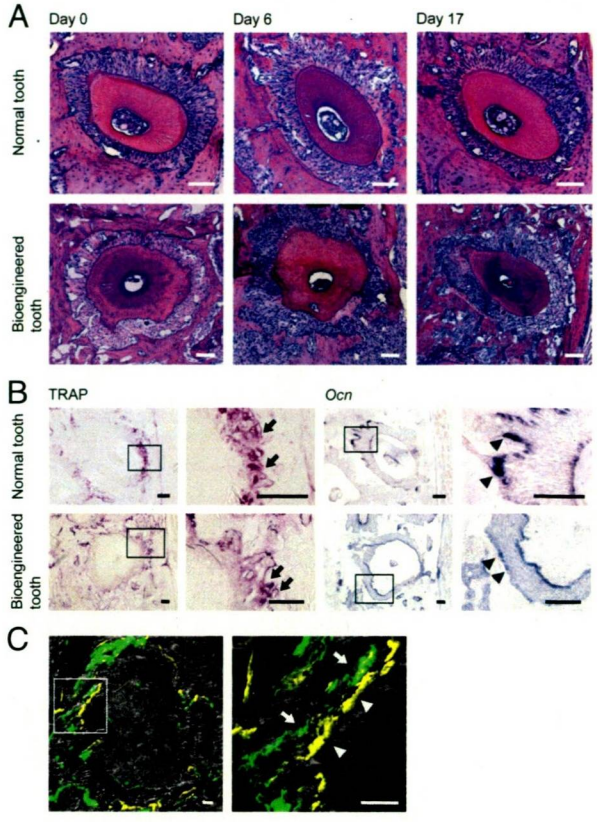

Fig. 3. Experimental tooth movement. (*A*) Horizontal sections of the root of a normal tooth (*Upper*) and a bioengineered tooth (*Lower*) were analyzed by hematoxylin-eosin staining (HE) at days 0 (*Left*), 6 (*Center*), and 17 (*Right*) of experimental orthodontic treatment. (Scale bar, 100 μm.) (*B*) Sections of a normal and bioengineered tooth were analyzed by TRAP staining and in situ hybridization of *Ocn* at day 6 of the orthodontic treatment. TRAP-positive cells (arrow) and *Ocn* mRNA-positive cells (arrowhead) are indicated. (Scale bar, 100 μm.) (*C*) The root of the bioengineered tooth was analyzed for bone formation. The image in the box in *Left* is shown at higher magnification in *Right*. Tetracycline (arrowhead) and calcein (arrow) labeling was detectable on the tension side. (Scale bar, 50 μm.)

alveolar bone, and suggesting that this tooth may be responsive to mechanical stress. It has been demonstrated previously that alveolar bone remodeling is induced via the response of the PDL to mechanical stress such as the treatment of orthodontic movements (31, 33). These same studies have further demonstrated that the localization of osteoclasts for bone resorption and osteoblasts for bone formation can be observed in the area of compression and on the tension side, respectively (31, 33). Thus, we analyzed the movement of our bioengineered tooth and also the osteoclast and osteoblast localization for remodeling in the alveolar bone by inducing orthodontic movements experimentally.

When the bioengineered tooth was moved buccally for 17 days with a mechanical force in an experimental tooth movement model, it performed as well as a normal tooth (Fig. 3*A* and Fig. S3). Histochemical analysis additionally revealed morphological changes in the PDL in both the sides containing lingual tension and buccal compression following 6 days of treatment (Fig. 3*A* and Fig. S3). Osteoblast-like cells, which have a cuboidal shape and rounded nuclei, and osteoclast-like cells, which are multinucleated giant cells, were observed on the surface of the alveolar bone within the tension and compression sides, respectively (Fig. 3*A* and Fig. S3). During experimental tooth movement, tartrate-resistant acid phosphatase (TRAP)-positive